Synthesis, Characterization, and Applications of Nanographene-Armored Enzymes

Maryam Khan, Qayyum Husain[1], Shamoon Asmat
Department of Biochemistry, Faculty of Life Sciences, Aligarh Muslim University, Aligarh, India
[1]Corresponding author: e-mail address: qayyumbiochem@gmail.com

Contents

1. Introduction 3
   1.1 Synthesis of Graphene-Armored Materials 4
   1.2 Functionalization of Graphene-Armored Materials 4
   1.3 Advantages of Using Graphene-Based Materials in Health-Related Applications 7
2. Facile Synthesis of Enzyme–Graphene-Armored Nanocomposites as Biocatalysts 8
3. Immobilization of the Enzyme Onto Graphene Anchored Nanocomposites 8
   3.1 Graphene–Iron Oxide NC 15
   3.2 Synthesis and Characterization of Gr@Fe_3O_4 NC 22
   3.3 Binding Studies of Immobilized β-Galactosidase 29
   3.4 Stability Studies of Immobilized β-Galactosidase 30
   3.5 Reusability and Storage Stability 32
   3.6 Toxicity Assessment 33
   3.7 Polyaniline-Coated Silver-Functionalized Graphene NC 35
   3.8 Characterization of Free and ANL Bound PANI/Ag/GONC 41
   3.9 Immobilization Efficiency of ANL@PANI/Ag/GONC 44
   3.10 Stability Studies of ANL@PANI/Ag/GONC 45
   3.11 Reusability Analysis of ANL@PANI/Ag/GONC 48
4. Summary and Future Outlook 48
Acknowledgments 51
Funding 51
References 51
Further Reading 60

Abstract

The unexpected discovery of graphene and especially the follow-up explosion of interest in its properties and applications marked the beginning of a new carbon era. Graphene-based nanostructured materials are highly useful because they show great promise in the field of biotechnology and biomedicine. Owing to their unique structural features, exceptional chemical, electrical, and mechanical properties, and their ability to

Methods in Enzymology
ISSN 0076-6879
https://doi.org/10.1016/bs.mie.2018.05.013

affect the microenvironment of biomolecules, graphene-armored nanomaterials are suitable for use in various applications, such as immobilization of enzymes, field-effect transistors, photovoltaic devices, and biosensors, which in turn is extremely vital to the development of biomedical instruments, clinical diagnosis, and disease treatment. In this chapter, we present our recently reported work to armor hydrolytic enzymes on graphene-based nanomaterial in order to develop novel scaffolds to build robust nanobiocatalysts. Synthesized graphene-Fe_3O_4 and polyaniline-coated silver graphene nanocomposite have been used to immobilize β-galactosidase and lipase, using noncovalent and covalent strategies, respectively. Herein, the methodologies of both techniques have been discussed in detail. Owing to the large surface area offered by the honeycomb like structure of graphene, very high amount of enzyme has been loaded on small amounts of the nanocomposite. The stability and reusability of the fabricated nanobiocatalysts have been compared with their free forms. Nanographene-armored enzymes demonstrated high catalytic stability and easy recovery from the reaction medium and can be applied in various biotechnological applications. Lastly, future prospects and possible challenges in this rapidly developing area have also been discussed.

ABBREVIATIONS

AChE	acetyl choline esterase
ADH	alcohol dehydrogenase
AFM	atomic force microscopy
AOx	alcohol oxidase
CNTs	carbon nanotubes
Cyt *c*	cytochrome *c*
DAOx	diamino oxidase
DLS	dynamic light scattering
EDS	energy dispersive X-ray spectroscopy
EDTA	ethylenediaminetetraacetic acid
FT-IR	Fourier-transform infrared spectroscopy
GO	graphene oxide
GOx	glucose oxidase
Gr	graphene
Gr@Fe_3O_4NC	graphene–iron oxide nanocomposite
Gr-NC	graphene nanocomposite
HRP	horseradish peroxidase
MNPs	magnetic nanoparticles
MP-11	microperoxidase-11
NC	nanocomposite
NM	nanomaterial
NPs	nanoparticles
ONPG	*o*-nitrophenyl β-D-galactopyranoside
PANI	polyaniline
PANI/Ag/GONC	polyaniline silver graphene oxide nanocomposite

p-NPP	*p*-nitrophenyl palmitate
PPO	polyphenol oxidase
RGO	reduced graphene oxide
Rh	hydrodynamic radius
SEM	scanning electron microcopy
TEM	transmission electron microscopy
Tyr	tyrosinase
VSM	vibrating sample magnetometer
XRD	X-ray diffraction

1. INTRODUCTION

Enzyme immobilization, a well-established and mature technology, leads to enhanced stability, facilitates reuse and easy separation from the reaction medium, thus allowing the modulation of catalytic properties of immobilized enzymes and creating robust biocatalysts suitable for their uses in various commercial applications (Al-Lolage, Meneghello, Ma, Ludwig, & Bartlett, 2017; Gomes et al., 2017; Husain, 2010; Husain & Qayyum, 2013; Husain & Ulber, 2011). The catalytic behavior of the enzyme is always affected by the nature of enzyme–support interactions and, thus, the availability of methods to immobilize enzymes with different materials is an important issue. Several approaches have been developed in the recent past for immobilization of enzymes (Ansari & Husain, 2012; Mateo, Palomo, Lorente, Guisan, & Lafuente, 2007; Sassolas, Blum, & Leca-Bouvier, 2012).

During the past 10 years, the synergistic interactions between nanotechnology and biotechnology have resulted in innovative functional biological nanosystems with potential applications in biotechnology, biosensing, and biomedical areas. Today, impressive achievements have been made at the cross-section of nanotechnology and biotechnology by employing modern nanomaterials (NM) to generate mechanical, optical, and electronic devices as well as biosensors (Husain, 2017a; Xiao, Bu, Yang, Zhang, & Xu, 2017; Yang et al., 2010). The development of effective nanobiocatalysts, in which enzymes are immobilized onto robust NM with tailor-made properties, is a typical example (Dutta, Biswas, & Saha, 2017; Husain, 2016, 2017b, 2017c).

Among the immobilization carriers used to date, nanostructured composite and hybrid materials, including metal oxide nanoparticles (NPs),

nanofibers, and carbon-based NMs are now under focus of intense fundamental and applied research (Ansari & Husain, 2012; Ge, Yang, Zhu, Lu, & Liu, 2012; Husain, 2018a; Verma, Barrow, & Puri, 2013). One of the most advantageous features of NM is their potential for manipulating the environment of biomolecules and thus, of their biological function and stability (Husain, 2017d; Rana, Yeh, & Rotello, 2010). The unique properties of NM as immobilization support is due to their extremely small size, together with other desirable properties, such as conductivity, large surface area to volume ratio, high catalytic efficiency and surface reactivity, strong adsorption ability and magnetism, and these offer particularly exciting opportunities for the preparation of effective nanobiocatalysts for the development of unique enzyme applications (Husain, 2017e, 2018b; Johnson, Park, & Driscoll, 2011; Verma et al., 2013).

1.1 Synthesis of Graphene-Armored Materials

There are different synthetic routes to produce graphene (Gr) materials with distinct properties for various potential bioanalytical applications. Currently, the most common method to obtain Gr is through the chemical reduction of exfoliated graphene oxide (GO) (Alsharaeh, Othman, & Aldosari, 2014; Takahashi, Abiko, & Anzai, 2013; Wei et al., 2010; Yang, Feng, Hong, Cai, & Liu, 2013). This is called reduced GO (rGO) or chemically derived Gr. In addition to mechanical exfoliation, GO can also be chemically, thermally, or electrochemically engineered to manipulate its optoelectronic properties (Liu & Ma, 2014; Shi et al., 2015) and produce Gr-based materials (Allen, Tung, & Kaner, 2010; Chen, Tang, & Li, 2010), including single-layer Gr, few-layer Gr, GO, thermally reduced GO, and electrochemically reduced GO. In contrast to pristine Gr, chemical vapor deposition growth can be used to obtain large Gr films and to introduce heteroatoms like nitrogen, boron, etc. (Liu et al., 2014; Sun et al., 2010). The choice of peculiar Gr material should be made according to the targets to be detected and the biorecognition mechanism to be utilized.

1.2 Functionalization of Graphene-Armored Materials

Gr-based NMs can be engineered for grafting desirable functional groups (such as epoxide, carboxylic, and hydroxyl groups) onto their surface providing functionalized NM with tailor-made properties and improved suitability for their application as nanoscaffolds (Dai, 2013; Loh, Bao,

Ang, & Yang, 2010; Wang, Li, Wang, Li, & Lin, 2011). This in turn, offers the possibility for introduction of functionalities that enhance fine-tuned actions of the immobilized enzymes such as protection from protease cleavage (Wang, Li, et al., 2011), enhancement of transportation capability in living cells (Sun et al., 2008; Wang, Zhang, et al., 2011), switchable activities responding to external signals (Cho, Kim, & Choi, 2013), facilitation of electron transfer to the protein (Kuila et al., 2011; Putzbach & Ronkainen, 2013; Walcarius, Minteer, Wang, Lin, & Merkoci, 2013), and lastly incorporation of enzymes in microdevices and microchip bioreactors (Bao, Chen, Zhang, & Chen, 2011; Liang, Wang, Liu, Meng, & Qiu, 2013).

To obtain Gr-based nanoprobes for molecular diagnostics, it is necessary to functionalize Gr with special elements that bring the detection targets onto the Gr surface through partial interactions and sometimes for signal amplification or transduction (Xu, Shen, Li, & Ye, 2014; Yu et al., 2014; Zhou et al., 2014). Moreover, chemical doping (Jiang et al., 2014; Yang et al., 2013) and surface functionalization (Yu, Dong, Zhang, Wang, & Zhi, 2014) are used to obtain Gr with better surface properties and improved dispersion. Frequently, metal NPs (e.g., Au, Ag, Pt, and Pd) can be decorated through electrochemical deposition, electrospray, or in situ reduction (Singh et al., 2014; Yang, Asiri, Du, & Lin, 2014). The oxygenated groups on the surface of both Gr and GO facilitate the nucleation of metal NPs. Then, metal ions are reduced to give metal NPs (Song et al., 2014; Zheng, Li, Li, & Chen, 2014) particularly, metal NPs decorated on Gr are synthesized following a bottom-up approach. Based on different immobilization techniques, the NPs can mediate signal transduction or anchor biomolecular probes with high capacity in Gr-based biosensors (She et al., 2014; Ye et al., 2014). After different modes of functionalization, Gr can be used in various strategies of molecular diagnostics.

GO is easily functionalized, thanks to its abundant oxygen containing groups (Georgakilas, 2012). Since, the first isolation of freestanding Gr sheets, this two-dimensional (2D) carbon crystal has been highly anticipated to provide a new and unique chance for bioanalytical applications. In fact, Gr has already shown great potential in preparing various novel nanoprobes based on its great electrical properties (e.g., high electron transfer rate), optical properties (e.g., outstanding ability to quench fluorescence), and structural properties (e.g., extremely high surface to volume ratio). The large 2D aromatic surface of Gr may also be functionalized in order to enhance its

bioanalytical properties (such as sensitivity, specificity, loading capacity, or biocompatibility), making it an ideal substrate for the synthesis and design of multicomponent nanoprobes (Pavlidis, Patila, Bornscheuer, Gounis, & Stamatis, 2014).

Various methods have been devised to functionalize Gr, including covalent methods, linker molecule mediating interaction, electrostatic interaction, and in situ synthesis of metal NPs. Chemical functional groups such as carboxylic (–COOH) and hydroxyl (–OH) groups can be covalently created on the Gr surface using strong acids and/or oxidants (Dai, 2013). In addition, microwave-assisted sulfonation has been used to create sulfonate ($–SO_3$) groups, while plasma (ammonia or nitrogen plasma) treatment has been used to create the amino ($–NH_2$) group on Gr (Choi et al., 2010). The grafting chemical moieties created on the Gr surface can serve as chemical handles for the conjugation of biological molecules (DNA, proteins, and carbohydrates) through covalent bonding (Wang, Li, et al., 2011). The properties, methods of functionalization, and various applications of Gr-based NMs have been summarized in Fig. 1.

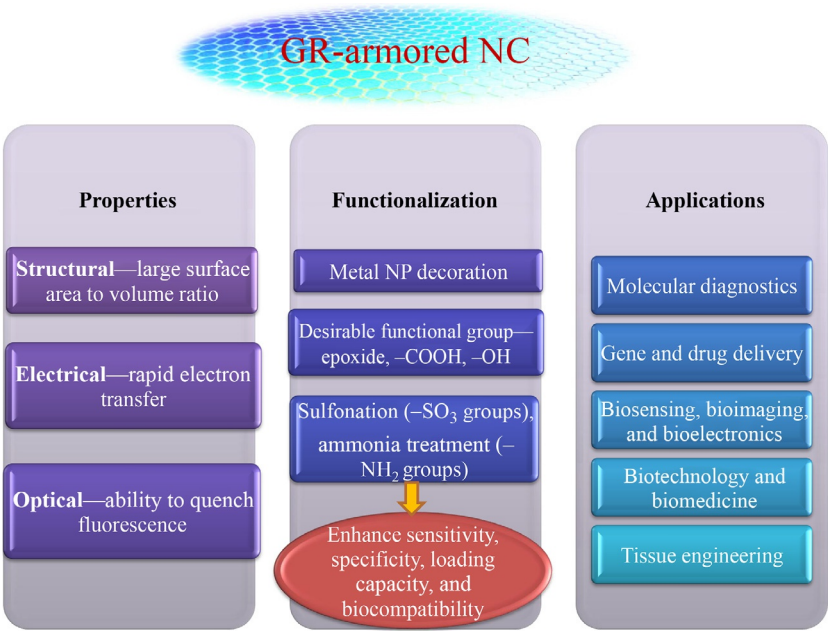

Fig. 1 Brief description of properties, ways of functionalization, and applications of Gr-armored NC.

Modification methods have also been developed to preserve the intrinsic properties of the original Gr materials. Gr can be viewed as the largest aromatic molecule. It can interact with some molecules by physical adsorption. For example, GO that is highly negatively charged, usually electrostatically adsorbs positively charged molecules. Additionally, van der Waals interaction or hydrophobic interaction may enhance the physical adsorption. Nevertheless, physical adsorption is not site specific. Thus, molecules (e.g., casein, BSA, and Tween-20) are often used to block the unwanted hydrophobic area in order to avoid nonspecific adhesion of nontarget molecules (Singh et al., 2014; Zhong et al., 2014). Graphene materials, particularly, GO and RGO, are useful materials for immobilizing NPs to exhibit better properties, such as higher conductivity, larger specific area, and remarkable thermal stability. By introducing metal NPs, metal oxides, or conductive polymers, the final Gr-based composite can achieve better catalytic and electrochemical activities for extending applications in biosensing. Several review articles have been published on Gr-based materials and their application in biosensing (Hernaez et al., 2017; Husain, 2017c; Yu et al., 2017; Zhu, Du, & Lin, 2017).

1.3 Advantages of Using Graphene-Based Materials in Health-Related Applications

Graphene and its derivatives play an ever-increasing role in the area of bioanalysis and biomedicine. In particular, they have been highly anticipated to provide new and unique opportunities for the improvement of novel nanoprobes for new biosensing methods and devices. Frequently, these new emerging nanoprobes have been applied in the areas related to human health such as diagnosis of viral diseases, nucleic acid mutations, and various cancers (Feng, Wu, & Qu, 2013; He, Zhang, Liu, Fang, & Zhang, 2014; Heldt et al., 2013). Till to date, the discovery of cancer diseases at an early stage is the most successful strategy to halt cancer progress by the detection of potential biomarkers. Thus, accurate, sensitive, and selective detection of nucleic acids, proteins, and small molecules is an urgent need due to their irreplaceable roles in human-related diseases (Zhu & Dong, 2014). GO has also been used as a photothermal agent for cancer treatment with encouraging therapeutic outcomes due to its high, intrinsic near-infrared (NIR) absorbance (Li, Yang, Ren, Qu, & Qu, 2012).

2. FACILE SYNTHESIS OF ENZYME–GRAPHENE-ARMORED NANOCOMPOSITES AS BIOCATALYSTS

This chapter deals with the fabrication of newly synthesized enzyme-Gr anchored NC for its possible applications in biocatalytic industry. The stable collaboration between nanosupports and biomolecules is of great importance to the area of nanobiotechnology. Based on the above-mentioned considerations, we chose *Aspergillus oryzae* β-galactosidase and *Aspergillus niger* lipase as model enzyme for the immobilization as they possess an intrinsic capacity to catalyze enantioselective hydrolysis, trans-esterification, esterification, and are extensively employed in the pharmaceutical, chemical, baking, food, textile, and biofuel industries, for the production of galactooligosaccharides, biochemical products, biosensors, paint, flavors, and biodiesel (Husain, 2016, 2017c). Nonetheless, despite its discernible intrinsic stability, the potential industrial applications of enzyme catalyzed reactions face frequent glitches, e.g., low stability and poor catalytic efficiency of enzyme, difficult retrieval of the enzyme from the reaction medium, lack of repetitive use, and the enzyme cannot be recycled. Thus, a fascinating approach to resolve the aforesaid snags is to immobilize the enzymes on different materials which includes NPs, NC, nanotubes, and layered double hydroxides. Additionally, the synthesis of numerous supports had led to the affordability of immobilized enzymes over a wider range of applications.

3. IMMOBILIZATION OF THE ENZYME ONTO GRAPHENE ANCHORED NANOCOMPOSITES

The discovery of Gr in 2004 added a new dimension to electrochemical biosensor research (Novoselov, Geim, & Morozov, 2004). Immediately after its isolation in 2004, this 2D material triggered scientific interest due to its extraordinary properties, which led to the Nobel Prize for Physics in 2010. The tremendous attention paid to Gr is based on its remarkable electrical, optical, and mechanical properties, such as large surface area, high electrical conductivity, excellent mechanical strength, and ease of functionalization (Geim & Novoselov, 2007). Despite its short history, and unique physicochemical properties, new Gr-based materials have made a profound impact in the fields of biotechnology and biomedicine, holding

Table 1 Various Gr-NC Bound Hydrolases and Their Potential Industrial Applications in Food Technology

Name of Enzyme	Name of NC	Application	References
Glucoamylase	GO/MNP-CC	Starch hydrolysis	Amirbandeh and Taheri-Kafrani (2016)
Amylase	MgNPs and GO	Application at very high temperatures	Dutta et al. (2017)
Cellulase	GO-MgNPs-	Enhanced hydrolysis of cellulosic compounds	Dutta, Biswas, and Saha (2016)
Cellulase	PEGylated GO	Enhanced straw hydrolysis	Xu et al. (2016)
β-Galactosidase	Gr@Fe_3O_4 NCs	Higher hydrolysis of lactose in batch processes	Khan, Husain, and Naqvi (2016)
Lipase	NH_2-GO and MWCNTs NC	Higher rate of esterification	Pavlidis et al. (2012)
Trypsin	GO-CO-NH-Fe_3O_4 NCs	Enhanced protein digestion efficiency and high throughput in proteomic study	Jiang et al. (2012)
Trypsin	GO-SiO_2 coated on PMMA	Highly efficient proteolysis in a microfluidic bioreactor	Bao, Zhang, and Chen (2013)
Trypsin	dGO nanosheets	High-throughput proteome identification	Jiang et al. (2014)

promising potential in applications such as in gene and drug delivery, bioremediation, bioimaging and biosensing, bioelectronics, tissue engineering and as antibacterial agents (Goenka, Sant, & Sant, 2014; Husain, 2017e; Krishna, Menard-Moyon, Verma, & Bianco, 2013). Table 1 summarizes various Gr-NC bound hydrolases and their potential industrial applications in food technology, while Table 2 depicts graphene nanocomposite (Gr-NC) bound enzymes and their application in the treatment of aromatic compounds from wastewater.

Table 2 Gr-NC Bound Enzymes and Their Environmental Application in the Treatment of Aromatic Compounds

Name of Enzymes	Type of NC	Compound Treated	References
Laccase	PAN/MMT/GO	Catechol	Wang et al. (2014)
Laccase	RGO/polymer GO nanoplatelets	RBBR	Ormategui, Veloso, Leal, Rodriguez-Couto, and Tomovska (2015)
Laccase	Carbon fullerene (C60), MWCNTs, *o*-MWCNTs, GO	Catechol and BPA	Pang, Li, and Zhang (2015)
Laccase	MGO	Decolorization of CV, MG, and BG	Chen et al. (2017)
Laccase	GO-$CuFe_2O_4$	Green synthesis of aryl sulfonyl benezenediols	Rouhani, Rostani, Salimi, and Pourshiani (2018)
Peroxidase	Co_3O_4-HRP/rGO/GCE	Chlorophenols	Chang et al. (2015)
Peroxidase	GO/Fe_3O_4 via EDC	Phenol, 95%	Chang, Huang, Ding, and Tang (2016)
Peroxidase	AuNPs/S-RGO	Bisphenol A	EzhiVilian et al. (2017)

The large surface area of Gr-armored NM creates an ideal immobilization support for various biomolecules including enzymes (Ge et al., 2012; Gokhale, Lu, & Lee, 2013; Lin et al., 2012; Pavlidis et al., 2012). The surface chemistry of these NM can influence their interactions with biomolecules and thus affect the adsorption as well as the conformational and biological function of conjugated proteins (Lin et al., 2012; Pavlidis et al., 2012). The large surface area and excellent electrical conductivity of Gr allows it to act as an "electron wire" between the redox center of an enzyme or protein and an electrode's surface. Rapid electron transfer facilitates accurate and selective detection of biomolecules with better sensitivity than conventional ones (Fig. 1). The addition of Gr leads to an increased sensing area and enhancement of the electron transfer rate (Zhang et al., 2016). Table 3 shows the list of various Gr-NC-based biosensors of oxidoreductive and hydrolytic enzymes, their analytes, linearity ranges of measurement and detection limits.

Table 3 Various Gr-NCs Based Biosensors of Oxidoreductive and Hydrolytic Enzymes, Their Analytes, Linearity Ranges of Measurement and Detection Limits

Name of Enzyme	Name NC	Analyte	Linearity Range	Detection Limit	References
ADH	AuNPs/PDA-RGO NC	Ethanol	5.0×10^{-8} to $4.2 \times 10^{-5} M$		Tian et al. (2013)
ChOx	Gr/PVP/PANI	Cholesterol	50 μM to 10 mM	1 μM	Ruecha, Rangkupan, Rodthongkum, and Chailapakul (2014)
Cyt *c*	GO-AuNPs-MWCNTS	Rebaudioside	0.001–0.05 mM	0.264 μM	Bathinapatla, Kanchi, Singh, Sabela, and Bisetty (2016)
DAOx	Gr–Pt NPs	Histamine	0.1–300 μM	$2.54 \times 10^{-8} M$	Apetrei and Apetrei (2016)
Laccase	RGO/Rh NCs GCE	17 β-estradiol	0.9–11 pM	0.54 pM	Povedano et al. (2017)
MP 11	Phospholipid-Gr-AuNPs	H_2O_2	2.0×10^{-5} to $2.8 \times 10^{-4} M$	$2.6 \times 10^{-6} M$	Wang, Liu, Ren, Wang, and Wang (2015)
HRP	AuPd-RGO-NW-PWE	H_2S	AuPd-RGO-NW-PWE		Yang et al. (2017)
PPO	PEDOT-RGO-Fe_2O_3-NCs GCE	Catechol	4×10^{-8} to $6.20 \times 10^{-5} M$	$7 \times 10^{-9} M$	Sethuraman, Mthuraja, Anandha, and Manisankar (2016)
Tyr	RGO-IrO_2NCs-SPE	Captopril	—	0.019 μM	Kurbanoglu, Rivas, Ozkan, and Merkoçi (2017)

Continued

Table 3 Various Gr-NCs Based Biosensors of Oxidoreductive and Hydrolytic Enzymes, Their Analytes, Linearity Ranges of Measurement and Detection Limits—cont'd

Name of Enzyme	Name NC	Analyte	Linearity Range	Detection Limit	References
Tyr	Gr-Au-CS-NC-SPCE	Phenolics	0.05–15 μ*M*	0.016 μ*M*	Fartas, Abdullah, Yusof, Sulaiman, and Saiman (2017)
GOx	MWCNT/GO hybrid biocomposite	Glucose	0.05–23.2 m*M*	28 μ*M*	Palanisamy, Karuppiah, and Chen (2014)
GOx	RGO/Ag NC electrode	Glucose	0.5–12.5 m*M*	0.16 m*M*	Palanisamy, Cheemalapati, and Chen (2014)
GOx	GO/lucigenin NC	Glucose	1.0×10^{-6} to 5.0×10^{-3} g mL^{-1}	9.9×10^{-7} g mL^{-1}	Gao, Zhang, and Cui (2014)
GOx	Gr-CNT-ZnO NC	Glucose	10 μ*M* to 6.5 m*M*	4.5 (±0.08) μ*M*	Hwa and Subramani (2014)
GOx	CSGr MNPs	Glucose	26 m*M*	16 μ*M*	Zhang, Chen, Ruo, Zhong, and Wu (2015)
GOx	PEI RGO-HAuNPs	Con A	1.0–20 ng mL^{-1}	0.31 ng mL^{-1}	Zhang et al. (2015)
GOx	Gr-CNTs	Glucose	2–8 m*M*		Terse-Thakoor, Komori, Ramnani, Lee, and Mulchandani (2015)
GOx	RGO nanosheets	Glucose	0.1–15.5 m*M*	5 μ*M*	Halder, Zhang, and Chi (2017)

GOx	RGO-Fe_3O_4 NC	Glucose	0.05–1 m*M*	0.1 μ*M*	Pakapongpan and Poo-Arporn (2017)
GOx	MRGO/PtAuNPs modified hybrid electrode	H_2O_2	0.5–8 m*M*		Hossain and Park (2017)
	CS-PDDA-MRGO/Pt AuNPs modified hybrid electrode	Glucose	0.01–8 m*M*	1 μ*M*	
AChE	Au-PPy-RGO NC-$(NH_4)_2SiF_6$	Paraoxon-ethyl	1.0 n*M* to 5 μ*M*	0.5 n*M*	Yang, Wang, Cao, Zhang, and Zhang (2014)
AChE	Gr-Au NCs GCE	Chlorpyrifos	0.05–150 $\mu g L^{-1}$	0.05 $\mu g L^{-1}$	Zhai, Guo, Sun, Zheng, and Wang (2014)
AChE	Cd0.5Zn0.5S-RGO NC	Acetylcholine	0.001–1 $\mu g mL^{-1}$	0.3 $ng mL^{-1}$	Liu, Zhang, Yan, Zhang, and Liu (2014)
AChE	Fe_2O_3NPs/RGO/PEDOT-FTO electrode	Acetylcholine	4.0 n*M* to 800 μ*M*	4.0 n*M*	Chauhan, Chawla, Pundir, and Jain (2017)
Urease	Sulfonated Gr/PANI NC	Urea	0.12–12.3 m*M*	0.050 m*M*	Das and Yoon (2015)

Modified from Husain, Q. (2017e). Biosensor applications of graphene–nanocomposites bound oxidoreductive and hydrolytic enzymes. *Analytical Methods, 9*, 6734–6746.

Lately, polymer–Gr composite supports have gained a lot of attention due to their characteristic properties such as low cytotoxicity, large surface area, lightweight, unique conjugated structure, better water dispersibility. Their functionalization for their applications in biomedicine, bioenergy, and nanobiotechnology is attractive. GO possess a 2D, single-layered sp^2 hybrid structure with adequate surface groups, offering an exceptional double sided, easily accessible substrate for multivalent functionalization and effective loading of molecules from small organic ones to biomacromolecules. Considering the binding between GO and biomacromolecules, such as enzymes, GO has been reported in numerous studies, typically for biosensing, as a support for immobilization of several enzymes, including horseradish peroxidase (HRP), glucose oxidase (GOx), amylase, β-galactosidase, and hemoglobin (Das, Talat, Srivastava, & Kayastha, 2018; Khan et al., 2016; Mansouri, Babadi, Bagheri, & Abd Hamid, 2017; Vineh, Saboury, Poostchi, Rashidi, & Parivar, 2018; Zhan, Tan, Wang, & Hou, 2018). Different oxidoreductive and hydrolytic enzymes immobilized on Gr-NC along with their industrial applications have been illustrated in Fig. 2.

In this chapter, we portray how the hydrolytic enzymes are amassed onto GO sheets to form graphene-armored nanobiocatalysts to further stabilize

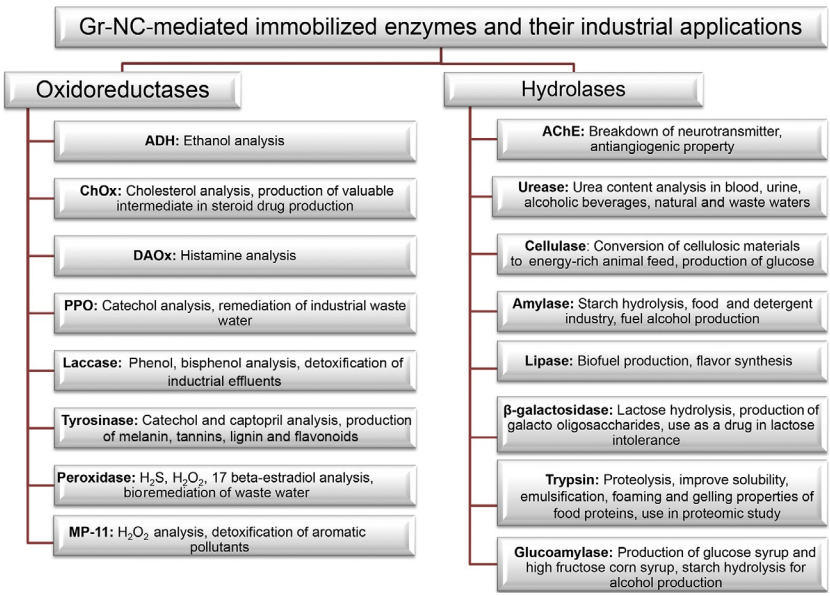

Fig. 2 Immobilization of enzymes onto Gr-armored NC and their industrial applications.

both β-galactosidase and lipase against denaturing environments while retaining their activities. Gr-iron oxide NC (Gr@Fe_3O_4 NCs) was synthesized using coprecipitation method, while the polyaniline-coated silver-functionalized GO anchored NC (PANI/Ag/GO NC) was prepared through in situ polymerization. β-Galactosidase was immobilized on Gr@Fe_3O_4NC employing physical adsorption; on the other hand, lipase was immobilized on PANI/Ag/GONC utilizing covalent method, protecting the enclosed enzyme while contributing fair access to the active site. The details of the characterization and fabrication are described in the subsequent sections. We state that the amalgamation of covalently immobilized enzyme with the polyaniline-coated silver-functionalized GO anchored NC boost the catalytic and operational stability of the biocatalyst even under severe conditions where native, undefended enzyme denatures. The outcomes displayed here completely support our claim, though simple and effective immobilization techniques and tools demand further exploration.

3.1 Graphene–Iron Oxide NC

3.1.1 Synthesis of Gr@Fe_3O_4 NC

General safety: Safety glasses, latex, or nitrile gloves, lab coat

Chemicals and reagents

1. Graphite—Sigma-Aldrich Chemicals Co., USA
2. $FeCl_2$—Sigma-Aldrich Chemicals Co., USA
3. $FeCl_3$—Sigma-Aldrich Chemicals Co., USA
4. NaOH—Merck & Co., USA

Equipment

1. Beaker (50–500 mL)
2. Stir/hot plate
3. Analytical balance
4. pH meter
5. Microtubes (1.5 mL)—Eppendorf, India
6. Magnet (6000G)
7. Magnetic stirrer with bar
8. Hot air oven

Methodology

GO was synthesized via modified Hummers method and was subsequently exfoliated by ultrasonication to attain an aqueous dispersion of

GO. Gr@Fe_3O_4 NC was synthesized by coprecipitating prehydrolyzed ferric and ferrous salts in the presence of GO (Zubir et al., 2014).

1. Prepare an aqueous solution (100 mL) containing $FeCl_3 \cdot 6H_2O$ (4.0 m*M*) and $FeCl_2 \cdot 4H_2O$ (2.0 m*M*) with an initial pH of 1.48.
2. Add GO solution (50 mL, 0.55 mg mL^{-1}) into the earlier mixture only when pH is adjusted to pH 4 via addition of NaOH (1.0 *M*) to prevent stacking of GO sheets at low pH.
3. Stir the solution for 30 min in order to obtain a stable and homogeneous mixture.
4. Now add NaOH (1.0 *M*) into mixture and during this process maintain the pH of solution at about 10.
5. Again stir the mixture constantly for 30 min at room temperature.
6. Separate the black precipitate, i.e., Gr@Fe_3O_4 NC from the reaction using a permanent magnet.
7. Once the magnetic nanoparticles (MNPs) are settled, wash them several times with deionized water and ethanol to remove any unbound and extra reagents.
8. Dry the precipitate well in a vacuum oven at 60°C for 48 h.
9. Also prepare pure Fe_3O_4 NPs via an analogous method without the addition of GO solution.
10. Store NC and NPs as a dried powder or as a suspension in deionized water or buffer until further use.

3.1.2 Characterization of Gr@Fe_3O_4 NC

General safety: Safety glasses, latex, or nitrile gloves, lab coat

Chemicals and reagents

1. Potassium bromide (AR Grade)—Sisco Research Laboratories (SRL), India
2. Sodium acetate (AR Grade) buffer (pH 4.5, 0.1 *M*)—SRL, India
3. Fe_3O_4 NPs and Gr@Fe_3O_4 NC (diluted solutions)

Equipment

1. Carbon-coated copper grids—300 mesh
2. JEOL-2100 transmission electron microscope, Japan
3. Sputter coater—JEOL JFC 1600, Japan
4. JSM-6510 LV scanning electron microscope, Japan
5. X-ray diffractometer (Rigaku, Japan-Miniflex-II)
6. BRUKER RFS 27: Stand alone FT-Raman Spectrometer
7. FT-IR Perkin Elmer instrument, USA (Spectrum-II, wave no. 4000-400)
8. Vibrating sample magnetometer (VSM, ADE EV5)

Methodology

The sizes and morphologies of Gr@Fe_3O_4 NC, Fe_3O_4 NPs and adsorbed β-galactosidase were examined by transmission electron and scanning electron microscopy (TEM and SEM), respectively.

1. Prepare small amounts of samples from Fe_3O_4 NPs, Gr@Fe_3O_4 NCs, and bound NC for TEM analysis by drop coating diluted solutions on carbon-coated copper grids at normal atmospheric conditions.
2. Analyze obtained samples under TEM at 200 kV.
3. Mount small samples from Gr@Fe_3O_4 NC, Fe_3O_4 NPs, and air dry immobilized enzyme on carbon tape on a copper stub, followed by 60 nm of gold deposition using a sputter coater.
4. Examine the samples under SEM at 15 kV. The crystal structure of the NPs and the NCs have been interpreted by X-ray diffraction (XRD) pattern obtained by X-ray diffractometer using a monochromatized X-ray beam with nickel-altered Cu Kα radiation. Keep scan speed of four steps per second with an angle range of 20–80 degrees.
5. The Raman spectra of Fe_3O_4 NPs and Gr@Fe_3O_4NC were recorded on a "Stand alone FT-Raman Spectrometer" using laser source Nd: YAG1064 nm and a resolution of 2 cm^{-1}. Fourier-transform infrared spectroscopy (FT-IR) spectra of the Fe_3O_4 NPs, Gr@Fe_3O_4 NC, and air dried immobilized enzyme were recorded using FT-IR Perkin Elmer Instruments, USA. Calibrate using polystyrene film and use KBr pellet method to run the samples. Acquire background spectra of clean atmosphere, prior to each sample measurement using identical acquisition parameters.
6. To assess the magnetic properties of Fe_3O_4 NPs as well as Gr@Fe_3O_4 NC wth a vibrating sample magnetometer (VSM) by measuring the applied field dependence of magnetization between −15,000 and 15,000 H (G) at room temperature. Lastly, the enzyme concentration was measured with the help of a UV–vis spectrophotometer.

The design of nanobiocatalyst by attaching β-galactosidase to Gr@Fe_3O_4 NC for scalable and reusable bio- and electrocatalytic applications is mentioned in the next section.

3.1.3 Immobilization of β-Galactosidase on Gr@Fe_3O_4 NC

General safety: Safety glasses, latex, or nitrile gloves, lab coat

Chemicals

1. Sodium acetate (AR grade) buffer (pH 4.5, 0.1 *M*)—SRL, India
2. Gr@Fe_3O_4NC (500 mg)
3. β-Galactosidase (*A. oryzae*)—Sigma-Aldrich Chemicals Co., USA

Materials and equipment

1. Falcons (15 mL)—Tarson, India
2. Microtubes (1.5 mL)—Eppendorf, India
3. Shaking incubator—Biogen. India
4. Micropipettes (20.0–100.0 μL, 0.1–1.0 mL)
5. Ultrasonicator—Life Care
6. Magnet (6000G)
7. UV–vis spectrophotometer (Shimadzu, UV-1800)
8. Centrifuge-REMI cooling centrifuge

Methodology

1. Independently adsorb free β-galactosidase on varying concentrations (ranging from 2 to 18 mg) of Gr@Fe_3O_4 NC by continuously shaking the mixture in sodium acetate buffer, pH 4.5 at 25°C.
2. Vary the enzyme concentration from 1 to 5 mg mL^{-1}, keeping the NC concentration (10 mg) fixed.
3. Also increase the immobilization time from 1 to 10 h.
4. Calculate the yield in all cases and take the highest yielding parameters to progress further.
5. Suspend and sonicate Gr@Fe_3O_4 NC (500 mg) in 0.1 *M* sodium acetate buffer, pH 4.5.
6. Load β-galactosidase (49.12 U) in the colloidal suspension.
7. Gently stir the mixture for 5 h and then either magnetically separate or centrifuge at 3000 × *g* for 10 min at 4°C.
8. The precipitate obtained is washed thrice with assay buffer and preserved at 4°C for further use.
9. Store the supernatant and the washes at 4°C for the calculation of immobilization yield.
10. Determination of immobilization yield.

The immobilization efficiency was determined in terms of immobilization yield as follows:

$$\text{Immobilization yield}(\%) = A - B/A \times 100\%$$

where *A* is the initially added activity of β-galactosidase/lipase in the immobilization system and *B* is the residual enzyme in the supernatant and washing solution after the immobilization process.

3.1.4 Stability Studies of Immobilized β-Galactosidase

Chemicals and reagents

1. β-Galactosidase—Sigma-Aldrich Chemicals Co., USA
2. Glycine–HCl (pH 2.0 and 3.0)—SRL, India

3. Sodium acetate buffer, pH (4.0, 4.5, and 5.0)—SRL, India
4. Sodium phosphate buffer, pH (6.0 and 7.0)—SRL, India
5. Tris–HCl buffer, pH (8.0 and 9.0)—SRL, India
6. Crushed ice
7. Galactose (1.0%–5.0%, w/v)—SRL, India
8. *o*-Nitrophenyl β-D-galactopyranoside, ONPG (0.1–1.0 m*M*)—SRL, India

Equipment

1. Water bath (30–110°C)—Scientech Instruments, Delhi
2. Ice maker and crusher—Labman
3. Ice box
4. Microtubes (1.5 mL)—Eppendorf, India
5. UV–vis spectrophotometer (Shimadzu, UV-1800)

Methodology

1. pH–activity profiles (Ansari & Husain, 2010)
   - **(a)** Prepare buffers of glycine–HCl (pH 2.0 and 3.0), sodium acetate (pH 4.0, 4.5, and 5.0), sodium phosphate (pH 6.0 and 7.0), and Tris–HCl (pH 8.0 and 9.0).
   - **(b)** Set the molarity of each buffer as 0.1 *M*.
   - **(c)** Incubate the free and immobilized enzymes in the buffers of different pHs.
   - **(d)** Consider the activity at pH 4.5 as control (100%) for the calculation of residual percent activity.
2. Temperature–activity profiles (Ansari & Husain, 2010)
   - **(a)** Incubate free and immobilized β-galactosidase (0.08 U) at different temperatures starting from 20 to 80°C in 0.1 *M* sodium acetate buffer of pH 4.5 for 15 min.
   - **(b)** Consider the enzyme activity at 50°C as control (100%) for the calculation of residual percent activity for free and immobilized enzyme.
3. Thermal denaturation (Ansari & Husain, 2010)
   - **(a)** Incubate free and immobilized β-galactosidase at 60°C in 0.1 *M* sodium acetate buffer, pH 4.5 for varying times.
   - **(b)** Take out aliquots of each preparation (20 mL) in triplicates at intervals of 15 min and chill them quickly in crushed ice for 5 min.
   - **(c)** Bring the enzyme to room temperature and perform assays as described earlier.
   - **(d)** Consider the activity of enzyme without incubation at 60°C as control (100%) for the calculation of residual percent activity.
4. Effect of galactose (Ansari & Husain, 2010)
   - **(a)** Incubate free and immobilized enzyme preparations (0.08 U) with various concentrations of galactose (1.0%–5.0%, w/v).

(b) Evaluate the activity of both enzymes in 0.1 *M* sodium acetate buffer, pH 4.6 at 37°C by performing enzyme assay.
(c) Consider the activity of enzyme without added galactose as control (100%) for the calculation of remaining percent activity.

5. Reusability of immobilized enzyme (Husain, Ansari, Alam, & Azam, 2011)
   (a) Take immobilized enzyme preparation (0.08 U) in triplicates for assaying the activity of the enzyme after repeated use.
   (b) Perform the reaction in 1.5 mL microtubes for 10 min at 37°C.
   (c) Immediately after incubation, centrifuge the mixture at 3000 × *g* for another 10 min at 4°C.
   (d) Decant the supernatant and add 0.1 *M* sodium carbonate into it, in order to stop the reaction.
   (e) After each assay, wash the immobilized enzyme with 0.1 *M* sodium acetate buffer, pH 4.5, by centrifugation at 3000 × *g* for 10 min.
   (f) Store the obtained pellet in assay buffer at 4°C and repeat this process for a period of 10 days.
   (g) Consider the activity determined on the first day as control (100%) for the calculation of residual percent activity after repeated use.
6. Storage stability of free and immobilized β-galactosidase (Ansari & Husain, 2010)
   (a) Store free and adsorbed β-galactosidase at 4°C in 0.1 *M* sodium acetate buffer of pH 4.5 for 2 months.
   (b) Take aliquots from each preparation (50 μL) in triplicates at a gap of 5 days and then analyze them for remaining enzyme activity.
   (c) The activity determined on the first day was considered as control (100%) for the calculation of residual percent activity.

3.1.5 Genotoxicity Assessment of Gr@Fe_3O_4 NCs

Reagents and chemicals

1. Histopaque-1077—Sigma-Aldrich Chemicals Co., USA.
2. RPMI-1640 medium—Sigma-Aldrich Chemicals Co., USA.
3. Low melting agarose—Sigma-Aldrich Chemicals Co., USA.
4. pBR^{322} DNA—Thermo Fischer Scientific, USA.
5. Ethylenediaminetetraacetic acid (EDTA)—SRL, India.
6. Tris—SRL, India.
7. Bromophenol Blue—Merck & Co., USA.
8. Glycerol—Merck & Co., USA.

9. Triton-X—SRL, India.
10. Ethidium bromide—Sigma-Aldrich Chemicals Co., USA.

Equipment

1. Beakers (500–1000 mL)
2. Incubator
3. Microtubes (1.5 mL) with stand—Eppendorf, India
4. Electrophoretic gel apparatus
5. UV-transilluminator
6. Fully frosted microscopic slides
7. Cover slips
8. Flat tray
9. Refrigerator
10. Ice packs

An image analysis system (Comet 5.5, Kinetic Imaging, Liverpool, UK) attached to an Olympus fluorescent microscope (CX 41, Olympus Optical Co., Tokyo, Japan) and a COHU 4910-integrated CC camera (equipped with 510–560 nm excitation and 590 nm barrier filters, COHU, San Diego, CA, USA).

Methodology

1. Plasmid nicking assay (Khan, Husain, & Ansari, 2013)
   - **(a)** Prepare a reaction mixture (30 mL) containing 10 m*M* Tris–HCl buffer, pH 7.5, pBR^{322} DNA (0.5 mg) with free enzyme (0.08 U), Gr@Fe_3O_4 NC (40 mg), and immobilized enzyme (10 mL) and incubate for 2 h at 37°C.
   - **(b)** Add 10 mL of solution containing 40 m*M* EDTA, 0.05% (w/v) bromophenol.
   - **(c)** Blue (tracking dye) and 50% (v/v) glycerol after incubation.
   - **(d)** Perform electrophoresis in submarine 1.0% (w/v) agarose gel.
   - **(e)** View and photograph ethidium bromide stained gel under a UV-transilluminator.
2. Comet assay (Khan et al., 2016)
   - **(a)** Use fully frosted microscopic slides precoated with 1.0% (w/v) normal melting agarose (PBS buffer lacking Ca^{2+} and Mg^{2+} ions).
   - **(b)** Mix diluted lymphocytes (10,000 cells) with 80 mL of 1.0% (w/v) low melting point agarose to form a cell suspension which is pipetted over the first layer and covered immediately by a cover slip.
   - **(c)** Put the slides on a flat tray and maintain on ice for 10 min to solidify agarose.

(d) Remove cover slips and layer 0.5% (w/v) low melting point agarose (80 mL). Allow to solidify on ice for 5 min.

(e) Remove the cover slips and within 20 min, treat cells with free enzyme (0.08 U), free NC (200 mg), and NC-adsorbed β-galactosidase (50 mL) for 1 h at 4°C.

(f) Perform all reactions on the slides in triplicates.

(g) Immerse the slides in cold lysis buffer containing 2.5 *M* NaCl, 100 m*M* EDTA, and 10 m*M* Tris–HCl, pH 10 for 1 h at 4°C and add 1% Triton-X 100 (just prior to use).

(h) After lysis, allow DNA to unwind for 30 min in an alkaline electrophoretic solution consisting of 300 m*M* NaOH and 1.0 m*M* EDTA, pH > 13.

(i) Run electrophoresis at 4°C in field strength of 0.7 V cm^{-1} and 300 mA current.

(j) Neutralize slides with cold 0.4 *M* Tris buffer, pH 7.5, and subsequently stain with 75 mL ethidium bromide (20 mg mL^{-1}) and cover with cover slips.

(k) Lastly, place the slides in a humidified chamber to prevent drying of gel and analyze the same day.

(l) Score comets at 100 × magnification. Analyze images from 50 cells (25 from each replicate slide).

(m) Tail length in millimeter (migration of DNA from the nucleus) is the parameter taken to assess DNA damage in human lymphocytes and it is automatically generated by the Comet 5.5 image analysis system.

3.2 Synthesis and Characterization of Gr@Fe_3O_4 NC

The synthetic methods for the preparation of Gr@Fe_3O_4 NC usually require tedious steps and toxic reagents such as hydrazine (Chandra et al., 2010) and $NaBH_4$ (Shin et al., 2009). Hence, there is an urgent need to develop a safe and efficient method to prepare Gr@Fe_3O_4 NCs. In this study, we have prepared Gr@Fe_3O_4 NCs by coprecipitation method and by employing eco-friendly reagents. Since pure Gr sheets have rare functional moieties on their surfaces, graphite oxide has appeared as a suitable substitute for Gr on account of having a large number of chemically reactive sites, such as epoxy and hydroxyl groups on the basal plane and the carboxylic groups at the surface (Fig. 3), and due to the presence of π–π conjugated system, which oxidizes Fe^{2+} ions for the nucleation and growth of Fe_3O_4 NPs (Yang et al., 2016).

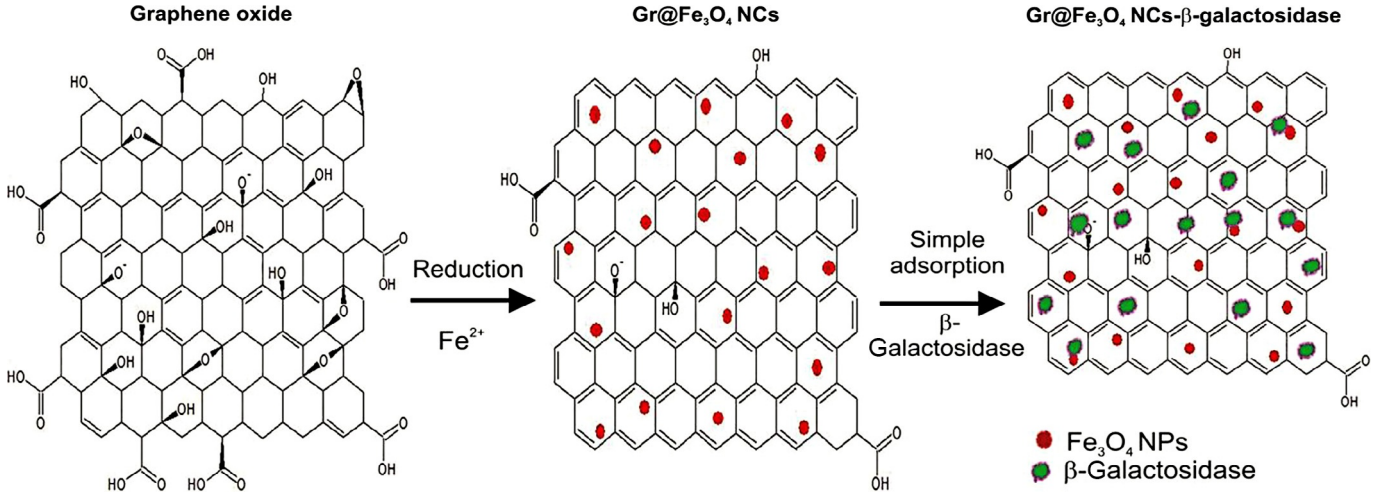

Fig. 3 Gr@Fe_3O_4 NC synthesis and immobilization of β-galactosidase on Gr@Fe_3O_4 NC. *Reproduced from Khan, M., Husain, Q., Naqvi, A. H. (2016). Graphene based magnetic nanocomposites as versatile carriers for high yield immobilization and stabilization of β-galactosidase.* RSC Advances, 6, *53493–53503.*

Fig. 3 depicts the procedure for the preparation of Gr@Fe_3O_4 NC and immobilization of β-galactosidase on Gr@Fe_3O_4 NC. Graphite oxide was reduced by the addition of Fe^{2+} ions which are attached to the surface of graphite oxide via electrostatic interactions and was oxidized to Fe^{3+} ions by the O^{2-} groups present on the surface of graphite oxide. NaOH was added in order to prevent restacking of graphite oxide sheets by increasing the pH of the medium. Consequently, the Fe^{2+} ions coprecipitated with the acquired Fe^{3+} ions into Fe_3O_4, leading to the formation of Gr@Fe_3O_4 NC (Yang et al., 2016). The enzyme was simply adsorbed on the surface of prepared NCs via hydrogen bonding and van der Waals interactions between the surfaces of protein and Gr@Fe_3O_4 NC (Khan, Qayyum, Alam, & Husain, 2011).

Free and β-galactosidase bound Gr@Fe_3O_4 NC were characterized by TEM, SEM, and FT-IR spectroscopy. XRD and VSM were carried out to monitor the crystallinity and confirm the magnetic character of the NPs and the NC, respectively. The surface morphologies and particle sizes of pure Fe_3O_4 NPs, Gr@Fe_3O_4 NC, and NC bound β-galactosidase were determined by using SEM and TEM. The incorporation of Fe_3O_4 NPs onto Gr sheets has been determined by TEM and SEM images (Fig. 4A–D). As seen in the representative TEM images of Gr@Fe_3O_4 NC. The surface of Gr was densely covered by cylindrical-shaped Fe_3O_4 NPs with an average size of about 25 nm (Fig. 4C and D). The distribution of Fe_3O_4 NPs on Gr sheet was evidently even, and no aggregation or large vacancy on Gr has been noticed. Fig. 4B and F illustrates the selection area electron diffraction (SAED) pattern of NC and Fe_3O_4 NPs, respectively. The observed NCs were found to be polycrystalline in nature with a slight visibility of circular rings while the Fe_3O_4 NPs were appeared crystalline in nature. He and Gao (2010) have also reported identical results. Fig. 4E and F demonstrates TEM and SEM images of Fe_3O_4 NPs. Roughly spherical Fe_3O_4 NPs are observed with an average particle size of 55 nm. The space resolved lattice fringes as shown in Fig. 4H agreed well with the lattice spacing planes of Fe_3O_4 NPs. In an earlier study also, similar findings have been described (Zubir et al., 2014).

The binding of β-galactosidase to the matrix has also been shown by SEM and TEM analyses. Fig. 5A and B clearly demonstrated the adsorption of protein onto functionalized Gr-NC. Rigid binding of enzyme to the support can be evidently illustrated by SEM analysis at 50, 10, and 5 mm

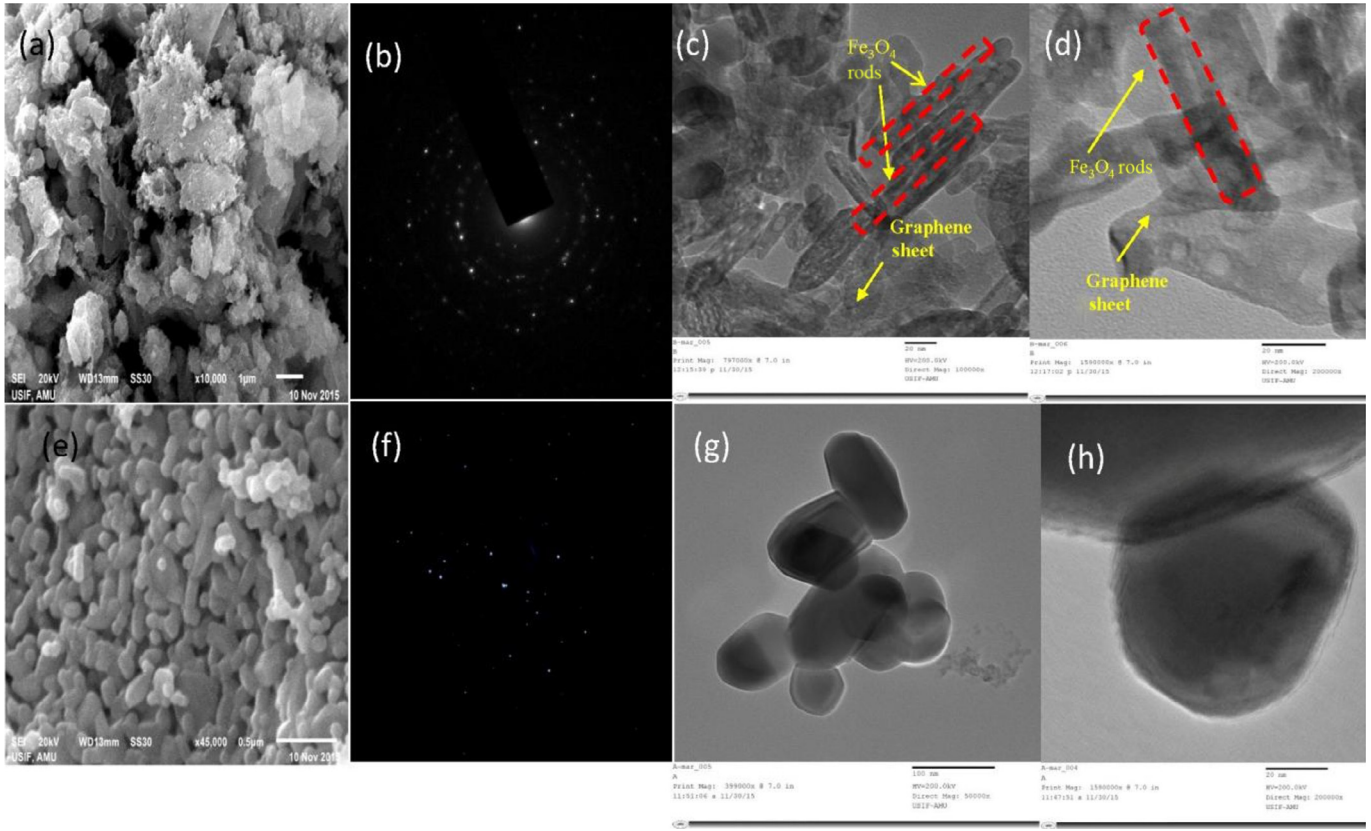

Fig. 4 (A) SEM image of Gr@Fe_3O_4 NC, (B) SAED pattern of Gr@Fe_3O_4 NC, (C and D) TEM images of Gr@Fe_3O_4 NC, (E) SEM image of Fe_3O_4 NPs, (F) SAED pattern of Fe_3O_4 NPs, (G) TEM image of Fe_3O_4 NPs, and (H) lattice fringes of a single Fe_3O_4 NPs. *Reproduced from Khan, M., Husain, Q., Naqvi, A. H. (2016). Graphene based magnetic nanocomposites as versatile carriers for high yield immobilization and stabilization of β-galactosidase.* RSC Advances, 6, *53493–53503.*

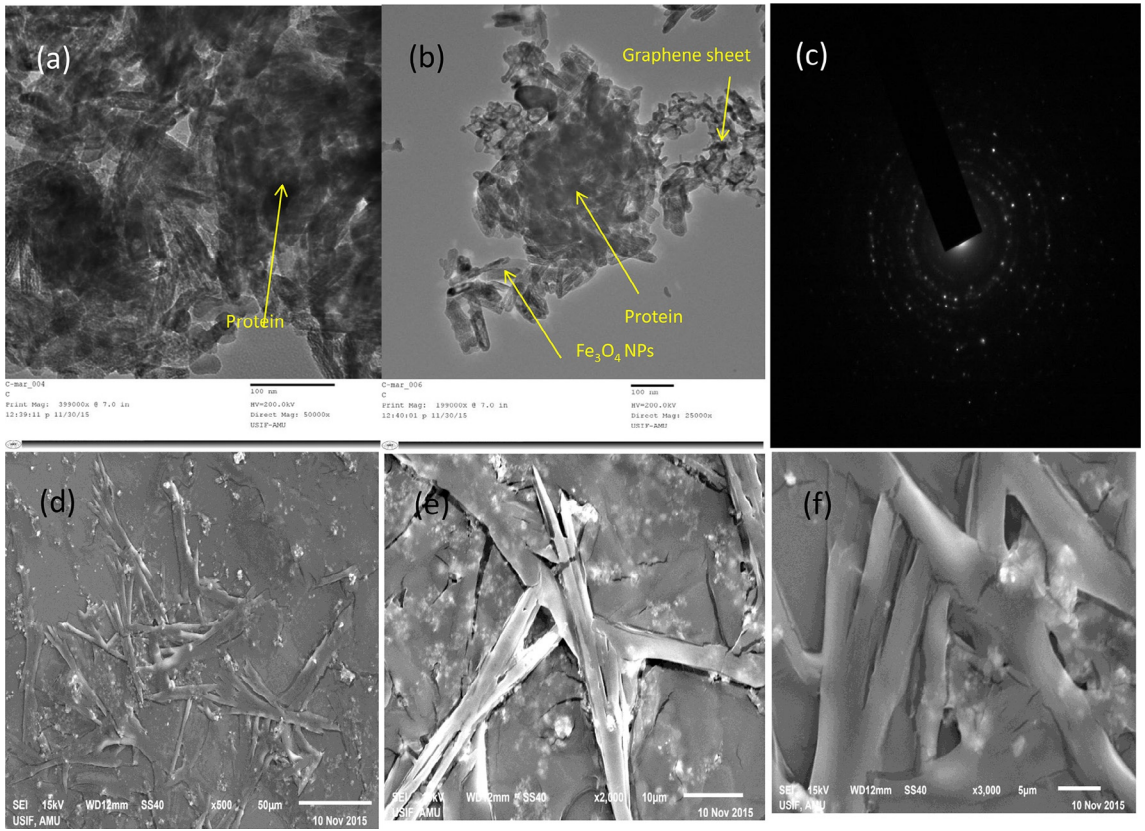

Fig. 5 TEM and SEM images of enzyme bound Gr@Fe_3O_4 NC (A and B) TEM images, (C) SAED pattern, and (D–F) SEM images at 50, 10, and 5 μm. *Reproduced from Khan, M., Husain, Q., Naqvi, A. H. (2016). Graphene based magnetic nanocomposites as versatile carriers for high yield immobilization and stabilization of β-galactosidase.* RSC Advances, 6, *53493–53503.*

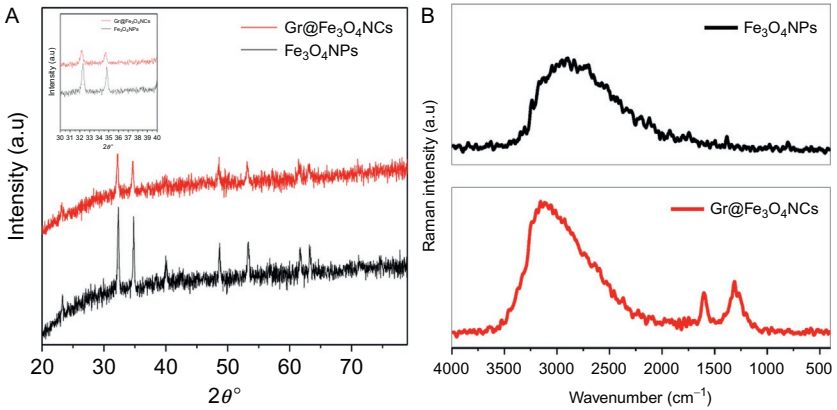

Fig. 6 (A) XRD pattern of Gr@Fe_3O_4 NC and Fe_3O_4 NPs and (B) FT-Raman spectra of Fe_3O_4 NPs and Gr@ Fe_3O_4 NC. *Reproduced from Khan, M., Husain, Q., Naqvi, A. H. (2016). Graphene based magnetic nanocomposites as versatile carriers for high yield immobilization and stabilization of β-galactosidase.* RSC Advances, 6, *53493–5350.*

(Fig. 5D–F), respectively. Moreover, the immobilization was also responsible for alteration in the characteristic SAED pattern. Fig. 5C shows distinguishable concentric rings which indicates that the Gr@Fe_3O_4 NC changes into highly crystalline form after binding with β-galactosidase.

Fig. 6A demonstrates XRD patterns for both Fe_3O_4 NPs and Gr@Fe_3O_4 NC. The crystallinity in both samples was corroborated by the presence of peaks at $2\theta = 32.31$, 34.65, 39.92, 48.71, and 53.26 degrees for Fe_3O_4 NPs and 32.49, 34.99, 40.14, 48.88, and 53.57 degrees for Gr@Fe_3O_4 NC, respectively. These peaks were found consistent with the standard XRD data in JCDPS (file no. 19-0629). No diffraction peak of other impurities is detected, demonstrating that both prepared sample are pure and crystalline in nature which was in accordance with the results reported earlier (Yang et al., 2016). Raman spectroscopic studies were also performed in order to assess the incorporation of Fe_3O_4 NPs on the Gr sheets. Fig. 6B illustrates the Raman spectra of Fe_3O_4 NPs and Gr@Fe_3O_4 NC. The Fe_3O_4 NPs spectrum showed a major peak at 2907 cm^{-1} and a small peak at 1382 cm^{-1}, corresponding to C—H and CH_3 bonding, respectively. The Raman spectrum of Gr@Fe_3O_4 NC revealed two prominent peaks at 1602 and 1310 cm^{-1} which demonstrated the presence of well-documented D (defects/disorder-induced modes) and G bands (in-plane stretching

tangential modes) in Gr sheets. The intensity ratio of D and G bands (ID/IG ratio) for GO was normally more than 1.0, as it was evidently recognized (Eigler, Dotzer, & Hirsch, 2012), but on reduction of graphite oxide to Gr in the presence of Fe^{2+} ions, the intensity ID/IG ratio was decreased to 0.82. Similar findings have also been previously mentioned by Narayanan et al. (2012) who synthesized and characterized rGO–Fe_3O_4 multifunctional freestanding membranes. These bands were not observed in Fe_3O_4 NPs. The peak at 1602 cm^{-1} further indicated the presence of aromatic ring chain vibrations (C═C) and showed attachment of Fe_3O_4 NPs to Gr sheets.

Fe_3O_4 NPs as well as the Gr@Fe_3O_4 NC were exposed to external magnetic field sweeping from −15,000 to 15,000 H (g) at room temperature by the use of VSM to assess their magnetic properties. Fig. 7A represents the magnetic hysteresis (M–H) loops of Gr@Fe_3O_4 NC and it exhibited an

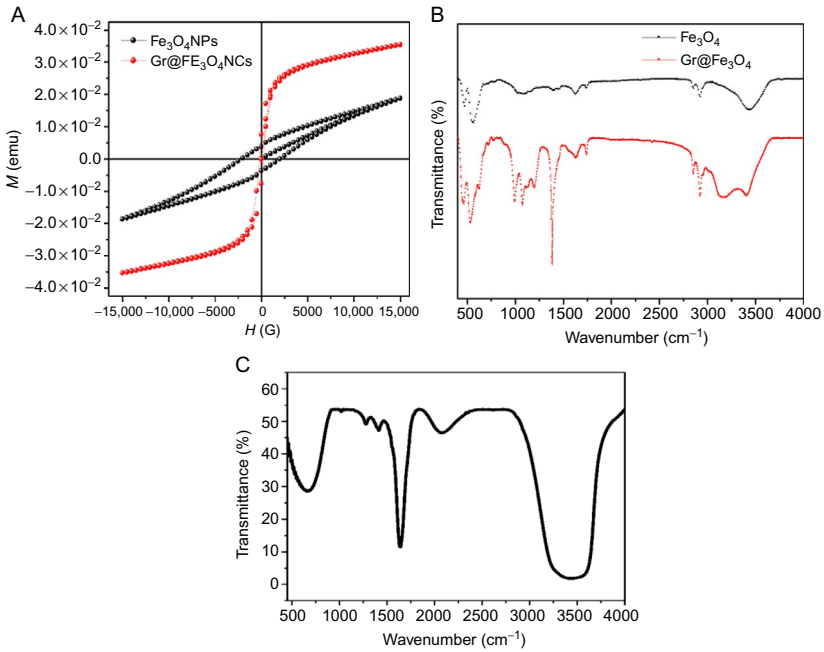

Fig. 7 (A) Magnetic hysteresis loops of Fe_3O_4 NPs and Gr@Fe_3O_4 NC measured at room temperature, (B) FT-IR spectra of Fe_3O_4 NPs and Gr@Fe_3O_4 NC, and (C) Enzyme bound Gr@Fe_3O_4 NC. *Reproduced from Khan, M., Husain, Q., Naqvi, A. H. (2016). Graphene based magnetic nanocomposites as versatile carriers for high yield immobilization and stabilization of β-galactosidase.* RSC Advances, 6, *53493–53503.*

S-shaped curve with negligible retentivity and coercivity indicating no remaining magnetization upon removal of external magnetic field (He & Gao, 2010). The NC, hence, exhibited superparamagnetic behavior while the naked Fe_3O_4 NPs showed paramagnetic behavior. The saturation magnetization (M_s) for Gr@Fe_3O_4 NC was noticed nearly two folds higher than that of the naked ones, suggesting that the particles are highly superparamagnetic, which is a characteristic of a ferromagnetic material. Fig. 7B demonstrates the characteristic FT-IR spectra of Fe_3O_4 NPs and of free as well as bound Gr@Fe_3O_4 NC. In the first two samples, the peaks at 568 and 534 cm^{-1}, respectively, correspond to the Fe–O vibrations related to the magnetite phase (Mahdevi et al., 2013). The peak at 1631 cm^{-1} in the absorption spectra of Gr@Fe_3O_4 NC is the characteristic peak for C═C demonstrating the presence of Gr. The peaks observed at 2925 and 2854 cm^{-1} in Fe_3O_4 NPs and Gr@Fe_3O_4 NC, respectively, were due to C—H stretching. The FT-IR bands corresponding to OH stretching mode were shifted to lower wave number in FT-IR spectra of Gr@Fe_3O_4 NC, 3407 cm^{-1} than the pure Fe_3O_4 NPs, 3435 cm^{-1} due to the interaction taking place between the NPs and the Gr sheets (Baby, Aravind, Arockiadoss, Rakhi, & Ramaprabhu, 2010). It demonstrated the role of O—H group during interaction of NPs and Gr. Fig. 7C depicts the absorption spectrum of the immobilized enzyme. The β-galactosidase peaks from 3320 to 3547 cm^{-1} confirmed enzyme binding with the support (Ansari & Husain, 2011a). Furthermore, the peak at 1636 cm^{-1} corresponding to N—H bend also ascertained the presence of amide band I.

3.3 Binding Studies of Immobilized β-Galactosidase

Although the preparation of carrier is quite important for enzyme immobilization and its performance, the selection and optimization of immobilization conditions are equally critical for immobilized enzyme to express its maximum activity. Therefore, three parameters affecting the immobilization of β-galactosidase, i.e., enzyme concentration, Gr@Fe_3O_4 NC concentration, and immobilization time have also been standardized in this study. After optimizing all conditions, maximum immobilization yield was obtained at 1 mg mL^{-1} of enzyme, 10 mg of Gr@Fe_3O_4 NC, and 5 h of immobilization time. Table 4 demonstrates the calculation of immobilization yield of β-galactosidase on Gr@Fe_3O_4 NC in terms of enzyme units (U). Consequently, the immobilization strategy achieved 90% yield after optimizing all the earlier factors.

Table 4 Immobilization of β-Galactosidase on Gr@Fe_3O_4 NCs

Enzyme: NCs (mg)	Enzyme Activity Loaded, *X* (U)	Enzyme Activity in Washes, *Y* (U)	Enzyme Activity Bound on Gr@Fe_3O_4 NCs		Immobilization Yield (%), *B*/*A*
			Theoretical $(X - Y) = A$	Actual/ Immobilized = *B*	
10:100	49.12	0.075	49.04	43.84	89.7

Each value represents the mean for three independent experiments performed in duplicates, with average standard deviations, ≤5%.

Reproduced from Khan, M., Husain, Q., Naqvi, A. H. (2016). Gr based magnetic nanocomposites as versatile carriers for high yield immobilization and stabilization of β-galactosidase. *RSC Advances, 6*, 53493–53503.

3.4 Stability Studies of Immobilized β-Galactosidase

3.4.1 *Effect of pH and Temperature on the Activity of Free and Immobilized β-Galactosidase*

The catalytic activity of enzyme depends on its conformational structure. Even a minor change in the native conformation of the protein may result in the loss of its catalytic activity (Husain et al., 2011). Fig. 8A illustrates the pH–activity profiles for free and Gr@Fe_3O_4 NC bound β-galactosidase. The free and immobilized enzyme exhibited identical pH–optima at pH 4.5. However, the immobilized enzyme showed a significant broadening in pH–activity profile and retained higher fractions of catalytic activity at both acidic and basic sides of pH optimum, compared to that of the native enzyme. Gr@Fe_3O_4 NC bound β-galactosidase retained 42% activity at pH 8.0 whereas free enzyme lost nearly 98% of its original activity under similar experimental conditions. The Gr@Fe_3O_4 NC after binding to the β-galactosidase protected its confirmation at the active site, thus, it retained remarkably higher activity when compared to that of the free form (Husain et al., 2011).

Fig. 8B demonstrates the temperature–activity profiles for the free and NC bound enzyme. The temperature optima for both free and immobilized β-galactosidase were found to be same at 50°C. The immobilized enzyme maintained greater fraction of catalytic activity at higher temperatures than the free β-galactosidase. Gr@Fe_3O_4 NC bound β-galactosidase preserved 71% of its initial activity at 70°C while its free form retained only 31% of its activity under identical exposure. Husain et al. (2011) in an earlier study also noticed similar findings. Soluble and ZnO-adsorbed β-galactosidase showed temperature optima at 50°C whereas ZnO–NP bound β-galactosidase exhibited broadening in temperature optima from 50 to 60°C. ZnO–NP bound β-galactosidase exhibited 74% activity at

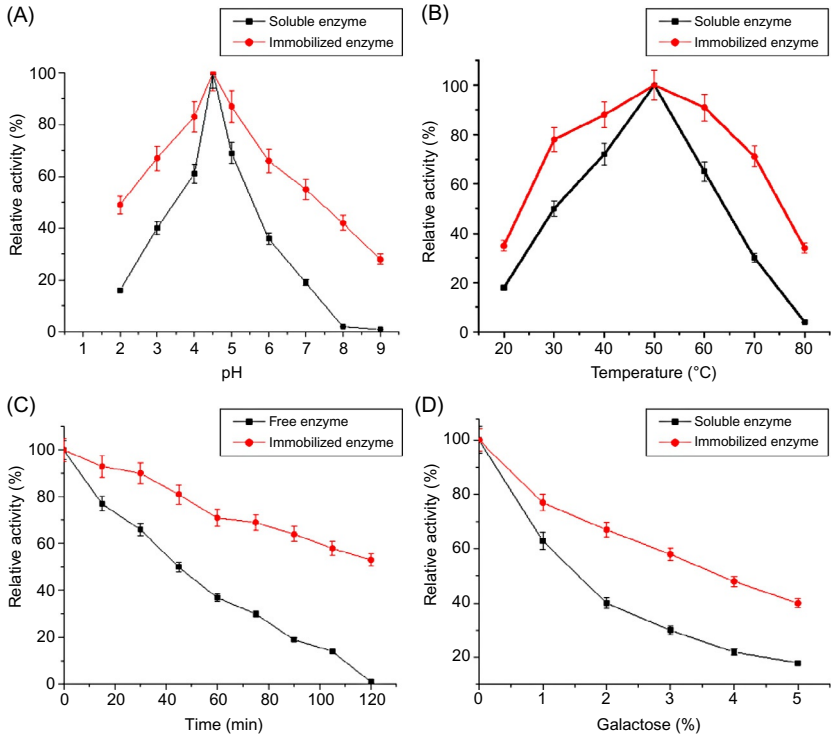

Fig. 8 (A) The pH–activity profiles for free and immobilized β-galactosidase. (B) Temperature–activity profiles for the free and immobilized β-galactosidase. (C) Thermal denaturation of the free and immobilized β-galactosidase. (D) Effect of galactose on the activity of the free and immobilized β-galactosidase. The activity of the enzyme in the absence of galactose was considered as control (100%) for the calculation of remaining activity at varying galactose concentrations. Data represent mean ± SD of three individual experiments performed in duplicates, p-value ≤ 0.05 for each figure. *Reproduced from Khan, M., Husain, Q., Naqvi, A. H. (2016). Graphene based magnetic nanocomposites as versatile carriers for high yield immobilization and stabilization of β-galactosidase.* RSC Advances, 6, *53493–53503.*

70°C while native ZnO-adsorbed and soluble enzyme retained only 58% and 31% activity under similar experimental conditions, respectively.

Gr@Fe_3O_4 NCs bound enzyme retained 53% of its initial activity, while the free enzyme lost almost its all activity under similar conditions. Husain et al. (2011) also demonstrated higher heat stability retained by the ZnO bound β-galactosidase compared to its free form under similar heat exposure. The loss in enzyme activity at higher temperatures might be due to denaturation of enzyme molecules. However, the immobilization matrix

provided rigidity to the enzyme structure and thus, it made the immobilized enzyme highly stable against inactivation mediated by heat treatment (Singh et al., 2014).

3.4.2 Effect of Galactose

Some earlier workers have reported that β-galactosidase can be competitively inhibited by its own product, galactose (Haider & Husain, 2007; Husain, 2010; Park & Oh, 2010). Therefore, an attempt has been made to evaluate the effect of galactose (1.0%–5.0%, w/v) on the activity of free and NC bound β-galactosidase (Fig. 8D). The findings showed that immobilized β-galactosidase appeared significantly more resistant to galactose-mediated inhibition, when compared to the soluble enzyme free form at varying concentrations. The immobilized β-galactosidase maintained 40% of its initial activity in the presence of 5% galactose, while the free enzyme retained only 18% of its activity under similar experimental conditions.

3.5 Reusability and Storage Stability

Reusability is one of the most important parameters to investigate the significance of immobilized enzyme in various sectors on large scale. Fig. 9A illustrates the residual activity of Gr@Fe_3O_4 NC bound β-galactosidase after repeated uses. The immobilized enzyme retained 80% of its activity after its ninth repeated use. The high operational stability of the bound enzyme can effectively reduce operational cost in practical applications. Leaching of the enzyme from the support was responsible for activity loss which is because of the weakening of the binding forces between matrix and enzyme during their reuses (Singh et al., 2014). The free and immobilized β-galactosidase preparations are stored at 4°C, and activity measurements are carried out at the gap of 5-day intervals for 60 days (Table 5). The Gr@Fe_3O_4 NC bound β-galactosidase exhibited markedly high stability than its free form. The immobilized enzyme retained 79% of its initial activity during storage, while the free β-galactosidase lost more than 50% of its activity under identical storage conditions. Several earlier investigators have also found an improvement in the stability of enzymes on very long storage. Improved storage stability of the immobilized enzyme has been reported by several earlier workers (Ansari & Husain, 2011b; Bayraktar, Serilmiz, Karakas, Celem, & Onal, 2011; Singh & Kayastha, 2012).

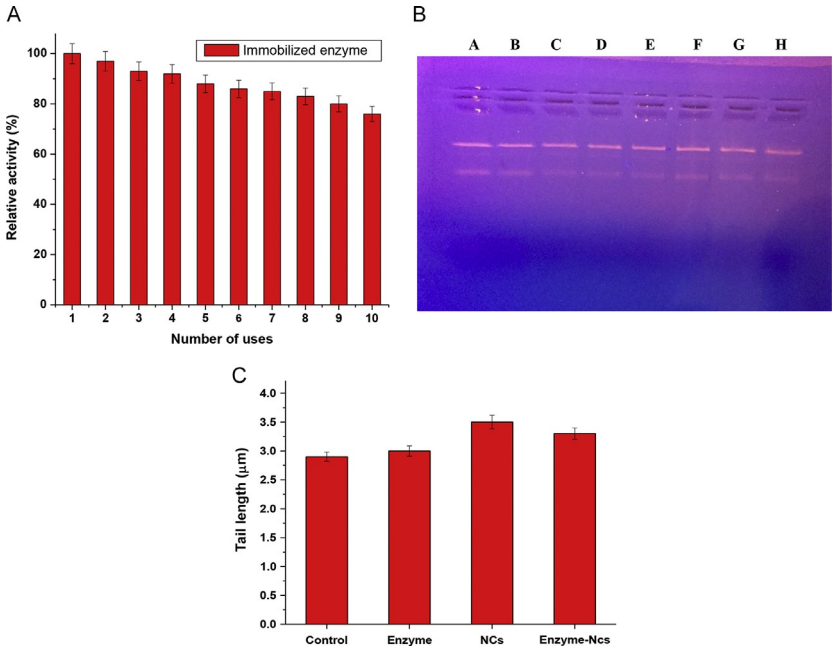

Fig. 9 (A) Reusability assay of immobilized β-galactosidase. The reusability of adsorbed β-galactosidase was monitored for 10 successive days. NC bound enzyme was taken in triplicates, and the activity determined on the first day was taken as the control (100%). *p*-Value ≤ 0.05 was considered statistically significant, (B) Plasmid nicking assay: Lanes A and B: pBR^{322} DNA alone, Lanes C and D: pBR^{322} DNA + enzyme (0.08 U), Lanes E and F: pBR^{322} DNA + $Gr@Fe_3O_4$ NC (40 μg), and Lanes G and H: pBR^{322} DNA + $Gr@Fe_3O_4$ NC bound β-galactosidase. (C) DNA damage in human lymphocytes by the enzyme alone (0.08 U), $Gr@Fe_3O_4$ NC (200 μg), and $Gr@Fe_3O_4$ NC bound enzyme. Data represent mean ± SD of three individual experiments performed in triplicates, *p*-value ≤ 0.05. *Reproduced from Khan, M., Husain, Q., Naqvi, A. H. (2016). Graphene based magnetic nanocomposites as versatile carriers for high yield immobilization and stabilization of β-galactosidase.* RSC Advances, 6, *53493–53503.*

3.6 Toxicity Assessment

It is essential to investigate the genotoxic effect of $Gr@Fe_3O_4$ NC in order to use it as an enzyme immobilization support for use in food technology. The plasmid nicking assay is one of the important parameters, which is used to evaluate the effect of various genotoxic chemicals on the integrity of DNA. In this study, pBR^{322} DNA was exposed to the enzyme alone, the $Gr@Fe_3O_4$ NC and NC bound β-galactosidase. Fig. 9B showed no damaging effect on the plasmid DNA, since the band intensity of the treated

Table 5 Storage Stability of Soluble and NC Bound β-Galactosidase Preparations When Kept at 4°C in 0.1 *M* Sodium Acetate Buffer, pH 4.5 for Over 60 Days

	Remaining Activity (%)	
Number of Days	**Free β-Galactosidase**	**Immobilized β-Galactosidase**
Control	100	100
5	94 ± 3.95	99 ± 4.98
10	87 ± 3.80	97 ± 4.85
15	84 ± 3.72	94 ± 4.70
20	76 ± 3.65	93 ± 4.65
25	72 ± 3.56	92 ± 4.62
30	67 ± 3.43	89 ± 4.45
35	63 ± 3.31	87 ± 4.35
40	62 ± 3.28	85 ± 4.27
45	60 ± 3.20	84 ± 4.19
50	56 ± 3.15	83 ± 4.05
55	52 ± 3.09	81 ± 3.96
60	49 ± 3.02	79 ± 3.88

The activity on first day was taken as control (100%) for the determination of remaining percent activity. p-Value ≤ 0.05 was considered statistically significant.

Reproduced from Khan, M., Husain, Q., Naqvi, A. H. (2016). Graphene based magnetic nanocomposites as versatile carriers for high yield immobilization and stabilization of β-galactosidase. *RSC Advances, 6*, 53493–53503.

sample was recorded similar to the control in all the cases. Ansari and Husain (2011a) have earlier also reported identical findings.

Single cell gel electrophoresis, commonly known as comet assay, is a very sensitive technique to assess DNA strand breaks in individual cells and has been recommended by various workers as a valid indicator for the examination of genotoxicity (Tice et al., 2000; Vnenchak & Rokosz, 1997). Human lymphocytic DNA of human lymphocytes was treated in vitro by free enzyme, the free Gr@Fe_3O_4 NC, and NC bound β-galactosidase, and the tail length, a parameter of DNA damage was plotted against concentration of different samples. Tail lengths obtained for lymphocytic DNA exposed to free enzyme, free Gr@Fe_3O_4 NC, and NC bound the β-galactosidase were found to be around 3.5 and 3.3 mm approximately, as compared to control (3.0 mm), it evidently demonstrates that the support

used in this study for immobilization of β-galactosidase is not toxic and highly biocompatible in nature (Fig. 9C). The toxicity assessment for any immobilized β-galactosidase system has been rarely reported. However, it is equally important to assess the toxicity of the support, because it can be applied at large scale in the food industry to give orally to the lactose intolerant people worldwide (Ansari & Husain, 2011a).

3.7 Polyaniline-Coated Silver-Functionalized Graphene NC

3.7.1 Synthesis of PANI/Ag/GONC

General safety: Safety glasses, Latex, or nitrile gloves, lab coat

Reagents and chemicals

Silver nitrate—Sigma-Aldrich Chemicals Co., USA
Graphite flakes—Sigma-Aldrich Chemicals Co., USA

Equipment

1. Beaker (50–500 mL)
2. Stir/hot plate
3. Analytical balance
4. pH meter
5. Microtubes (1.5 mL)—Eppendorf (India)
6. Magnet (6000G)
7. Magnetic stirrer with bar

Methodology

The PANI/Ag/GONC was synthesized through in situ polymerization procedure. To be precise, following steps were taken in order to successfully synthesize the above-mentioned NC. Formulation of Gr hybrid support involved the preparation of GO solution from graphite. Preparation of GO is outlined later:

1. Add potassium persulfate (0.1 *M*) into 10% aniline solution under constant stirring conditions at very low speed in the molar ratio of 1:1 for 3 h.
2. Now add ammonium persulfate solution dropwise to the aniline solution in 1 *M* HCl and keep for 45 min under constant stirring condition. A dark green colored precipitate is obtained which indicates successful formation of PANI.
3. Prepare 2 m*M* of silver nitrate in Tris–HCl buffer, pH 8.5 and add this slowly drop by drop to the as prepared PANI solution. Gently stir for 2 h in an ice bath.
4. Synthesize GO via oxidative treatment of natural graphite flake utilizing a modified "Hummers method" following ultrasonication treatment for 1 h.

5. Add GO to solution comprising PANI/Ag and actively stir in a water bath containing ice for 2 h and keep the obtained solution in a refrigerator overnight at 4°C.
6. Wash the obtained prepared product many times with distilled water and ethanol.
7. Finally, air dry in the hot incubator at 60°C for 20 h and preserve it for further use.

3.7.2 Characterization of PANI/Ag/GONC

General safety: Safety glasses, latex, or nitrile gloves, lab coat

Chemicals and reagents

1. Potassium bromide
2. Sodium acetate buffer (pH 4.5, 0.1 *M*)
3. ANL@PANI/Ag/GONC (diluted solutions)

Equipment

1. UV/vis JASCO Spectrophotometer, Japan
2. Carbon-coated copper grids—300 mesh
3. Sputter coater—JEOL JFC 1600, Japan
4. Perkin Elmer FT-IR spectrometer, Spectrum Two, CT, USA
5. Perkin Elmer Pyris Thermogravimetric Analyzer, USA
6. JEOL-2100 100/120 kV Transmission Electron Microscope, JEOL, Tokyo, Japan
7. JSM 6510LV Scanning Electron Microscope, JEOL, Tokyo, Japan
8. Oxford Instruments INCAx sight EDAX spectrometer
9. Atomic Force Microscopy (AFM) Probe (RTESP, Veeco model Icon with controller and Nanoscope 5 integrated system)
10. DynaPro-TC-04 Dynamic Light Scattering (DLS) equipment (Protein Solutions, Wyatt Technology, Santa Barbara, CA) equipped with a temperature-controlled microsampler

3.7.2.1 Fourier-Transform Infrared Spectroscopy

FT-IR analysis was carried out in order to determine the interactions of enzyme with NC.

Methodology

1. Use Perkin Elmer FT-IR Spectrometer, Spectrum Two (CT, USA) for analyzing the interactions of the functional groups between the enzyme and NC.
2. Dilute all with spectroscopic grade potassium bromide to fix the samples in a clearer sheet for FT-IR measurements.

3. Record the spectra in a wavenumber range of 4000–400 cm^{-1} for the samples.
4. Take the average value of 12 scans for the samples.

3.7.2.2 Transmission Electron Microscopy

TEM analysis is basically done to understand the size and morphology of the synthesized NC as well as the nanobiocatalyst.

Methodology

1. Prepare aqueous samples of ANL and ANL@PANI/Ag/GONC making the concentration of about 0.1 m*M*.
2. Ultrasonicate the samples to make the mixture homogenously distributed.
3. Using a micropipette drop-cast 10 μL of the sample on the copper grid.
4. Now using filter paper blot the excess solution.
5. Dry the aliquots and record images using TEM instrument at accelerating voltage of 200 keV.

3.7.2.3 Scanning Electron Microscopy and Energy Dispersive X-Ray Spectroscopy (EDS)

SEM studies were performed to analyze the surface morphology of the synthesized NC before and after conjugation with lipase while EDS was employed to analyze the elemental composition of synthesized NC.

Methodology

1. Prepare aqueous samples of ANL and PANI/Ag/GONC bound ANL and ultrasonicate them for even distribution.
2. Using a micropipette drop-cast 10 μL of the sample on a glass cover slip and blot excess solution using filter paper.
3. Use JSM SEM instrument to record images.
4. Using INCAx sight EDAX spectrometer, elemental composition of NC was analyzed.

3.7.2.4 AFM

The tapping mode in AFM was employed to visualize roughness of the NC surface before and after immobilization of lipase.

Methodology

1. Dilute and ultrasonicate all the samples to around 0.1 m*M* concentrations.
2. Load 0.2 mL solution on the cover glass slit using a micropipette.

3. Use RTESP, Veeco model microscope and set resonance frequency and amplitude to 340 Hz and 13 mV, respectively.
4. Carry out microscopic scans on variable surface locations of the samples and record the AFM images.

3.7.2.5 DLS Measurements

DLS studies were carried for size distribution analysis of synthesized NC before and after conjugation with the enzyme.

Methodology

1. Dilute the samples to 0.01 m*M* equivalent enzyme concentration and ultrasonicate them for uniform distribution of the particles.
2. Use DynaPro-TC-04 DLS instrument and set the wavelength to 830 nm for executing size distribution analysis of the samples.
3. Record the DLS measurement outcomes at 830 nm wavelength.
4. For each experiment, take around 20 measurements and analyze the mean hydrodynamic radius (Rh) and polydispersity index using Dynamics 6.10.0.10 software.

3.7.3 Immobilization of Lipase on PANI/Ag/GONC (Zhu & Sun, 2012)

General safety: Safety glasses, latex, or nitrile gloves, lab coat

Chemicals

1. Tris buffer (pH 7.0, 20 m*M*) and sodium phosphate buffer (pH 7.4, 25 m*M*)
2. PANI/Ag/GONC (500 mg)
3. Lipase (*A. niger*)

Materials and equipment

1. Falcons (15 mL)—Tarson, India
2. Microtubes (1.5 mL)—Eppendorf, India
3. Shaking incubator—Biogen, India

Methodology

The above-mentioned GO anchored nanosupport was used to make hybrid enzyme–NC biocatalyst. The typical protocol for the synthesis of biocatalyst is as follows:

1. For analyzing optimum conditions aiming to maximum yield immobilization of enzyme onto the GO anchored NC, during immobilization of native *A. niger* lipase (ANL), vary concentrations of PANI/Ag/GO NC (5–20 mg) and concentrations of crosslinker for different time intervals.
2. Dissolve the earlier formulations in 50 m*M* phosphate buffer, pH 7 at 30°C.

3. Ultrasonicate GO-based NCs for 30 min.
4. Activate the amino groups of above-mentioned support with specific glutaraldehyde (crosslinker) concentration for different time periods from 2 to 12 h.
5. Wash the NC several times with double distilled water to eliminate unbound glutaraldehyde.
6. Dry in hot air incubator at 60°C.
7. Now, dissolve free ANL (10 mg) in 100 mL sodium phosphate buffer, pH 7.0 and add this slowly to a certain amount of PANI/Ag/GONC.
8. Stir the reaction mixture (180 rpm) on a magnetic stirrer for a specified time and isolate the immobilized preparation of Gr-armored enzyme nanobiocatalyst via centrifugation.
9. Remove the uncrosslinked lipase by washing till no protein is spotted and perform activity assay in order to detect the amount of uncrosslinked ANL.
10. Store the immobilized biocatalyst in assay buffer at 4°C for further experiments.

3.7.4 Activity and Stability Studies of ANL@PANI/Ag/GONC

Reagents and chemicals

1. *p*-Nitrophenyl palmitate (*p*-NPP)—Sigma-Aldrich Chemicals Co., USA
2. Sodium phosphate buffer (20 m*M*, pH 7.4)—SRL, India
3. Triton X-100—SRL, India
4. Tris–HCl buffer (25 m*M*, pH 7.0)—SRL, India
5. Acetone—SRL, India
6. Acetonitrile—SRL, India
7. Isopropanol—SRL, India
8. Butanol—SRL, India
9. Nitroaniline—SRL, India
10. Toluene—SRL, India
11. Chlorobenzene—SRL, India

Equipment

1. Water bath (30–110°C)—Scientech Instruments, India
2. Ice maker and crusher—Labman, India
3. Ice box
4. Microtubes (1.5 mL)—Eppendorf, India
5. UV–vis spectrophotometer—Shimadzu, UV-1800, Japan)

Methodology

1. Use UV Spectrophotometer (JASCO) to determine catalytic activity of the samples using hydrolysis assay.
2. Prepare the samples of soluble and immobilized enzyme of equal enzyme concentration, i.e., $1\,mg\,mL^{-1}$.
3. Prepare stock solution of lipase ($1\,mg\,mL^{-1}$) in 50 m*M* phosphate buffer, pH 7.0.
4. Prepare substrate solution with *p*-NPP (150 m*M* in isopropanol), 150 mL Triton X-100, and 67.5 mL 25 m*M* Tris–HCl buffer, pH 7.0. The reaction mixture consisted of 2 mL substrate and 0.1 mL lipase solution.
5. Incubate free and immobilized lipase independently (6.2 U), in appropriate buffers of varying pH; sodium acetate (pH 4.0–5.0), sodium phosphate (6.0 and 7.0), and Tris–HCl (pH 8.0, 9.0, and 10.0) and perform hydrolysis assay to determine the catalytic activity of the enzyme.
6. To evaluate the optimum temperature of the enzyme, incubate equal amounts of free and immobilized lipase at various temperatures (25–55°C) in 50 m*M* sodium phosphate buffer, pH 7.0 for 10 min and measure the *p*-NPP hydrolytic activity by both enzyme preparations.
7. To perform hydrolysis assay, incubate the reaction mixture at 37°C for 15 min in a water bath under continuous stirring condition, and add 0.25 mL 0.1 *M* Na_2CO_3 in order to terminate the reaction.
8. To analyze the thermal stability of both the free and immobilized lipase preparations, incubate both enzyme preparations simultaneously in 50 m*M* sodium phosphate buffer, pH 7 at 60°C for 2 h. Withdraw specific aliquots from both enzyme preparations at definite time intervals and chill them quickly in crushed ice for 5 min. The samples are then brought to room temperature until enzyme assay is performed.
9. For storage stability analysis, incubate the samples at 4 and 30°C in 2 mL of 50 m*M* sodium phosphate buffer, for a period of 30 days.
10. For solvent stability studies, incubate free ANL, and ANL@PANI/Ag/GONC (6.2 U) in 100 μL (33%, v/v) of various solvents such as nitroaniline, toluene, acetone, isopropanol, acetonitrile, butanol, and chlorobenzene at 30°C for 1 h. Also, incubate the obtained nanobiocatalyst in 0.05 *M* sodium phosphate buffer, pH 7.0 for the reference point in determining the effect of organic solvents.

3.7.5 Reusability Assay

1. Perform reusability assay of synthesized nanobiocatalyst-ANL@PANI/Ag/GONC (6.2 U) in triplicates in 50 m*M* sodium phosphate buffer, pH 7.0 for 11 successive cycles.
2. After each repetitive use, wash ANL@PANI/Ag/GONC with 50 m*M* sodium phosphate buffer, pH 7.0 and remove the pellet by centrifugation at 5000 × *g* for 10 min and store in assay buffer at 4°C.
3. The activity obtained on the first day was considered as control (100%), for the calculation of remaining percent activity after each repetitive use.

3.8 Characterization of Free and ANL Bound PANI/Ag/GONC

Fig. 10 illustrates SEM and TEM microphotographs of PANI/Ag/GONC and ANL@PANI/Ag/GONC. The morphology of the NCs before and

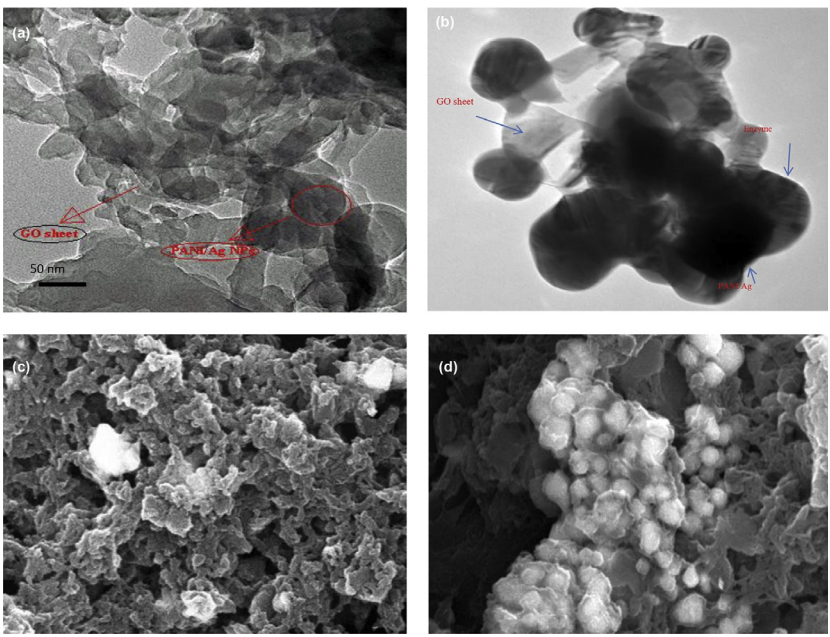

Fig. 10 Transmission electron micrographs of (A) PANI/Ag/GONC and (B) ANL@PANI/Ag/GONC. Scanning electron micrographs of (C) PANI/Ag/GONC and (D) ANL@PANI/Ag/GONC. *Reproduced from Asmat, S., Husain, Q., & Azam, A. (2017). Lipase immobilization on facile synthesized polyaniline-coated silver-functionalized graphene oxide nanocomposites as novel biocatalysts: stability and activity insights.* RSC Advances, *7(9), 5019–5029.*

after binding to the enzyme was affirmed and monitored by these techniques. The results showed that the NC are spherical in shape having a mean particle size of 50 nm and validate the capability of GO nanosheets to attach with PANI-coated Ag-NPs on their surface. The NC remained spherical in shape even after conjugation with ANL, however, the average diameter hiked from 50 to 72 nm, it signified that certain aggregation due to overlapping of some bigger particles with the smaller ones. The results showed the binding of considerable amounts of enzyme on the NC surface and demonstrated that the armoring of lipase with PANI/Ag/GONC did not alter the morphology of the NPs. Our findings are inconsistent with earlier reported results where the investigators have used Au/NP@Fe_3O_4 NPs as an immobilization support (Cao, Wen, Svec, Tan, & Lv, 2016).

To further affirm the morphology of the NC in these micrographs, AFM was performed to analyze the peak to peak valley distance in microphotographs as a pointer for the roughness in the surface of NC before and after immobilization of enzyme. As evident from Fig. 11, the NC surface before enzyme immobilization showed smaller peak-to-valley distance and was comparatively smooth, while after conjugation of enzyme with the NC was conjugated, there was a noticeable surge in peak-to-valley distance which demonstrated high enzyme loading. FT-IR was employed to

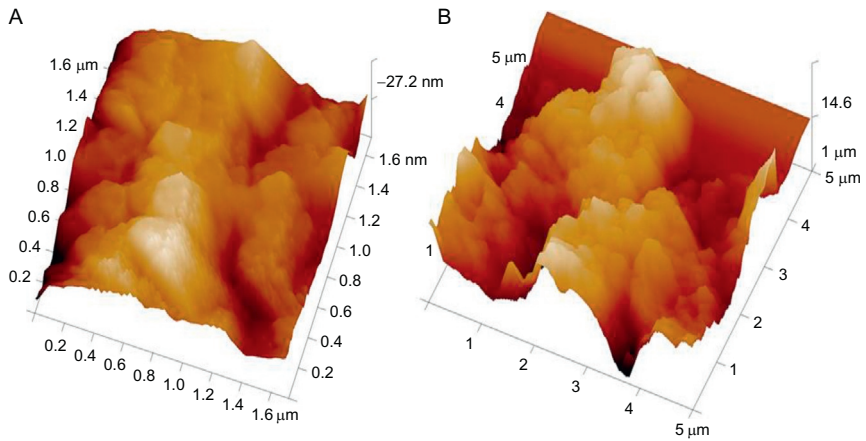

Fig. 11 Atomic force micrographs of (A) PANI/Ag/GONC and (B) ANL@PANI/Ag/GONC. Tapping mode of AFM is performed using commercial etched silicon tips as AFM probes with distinctive resonance frequency of c. 340 Hz and 13 mV amplitude (RTESP, Veeco, Japan). *Reproduced from Asmat, S., Husain, Q., & Azam, A. (2017). Lipase immobilization on facile synthesized polyaniline-coated silver-functionalized graphene oxide nanocomposites as novel biocatalysts: stability and activity insights.* RSC Advances, *7(9), 5019–5029.*

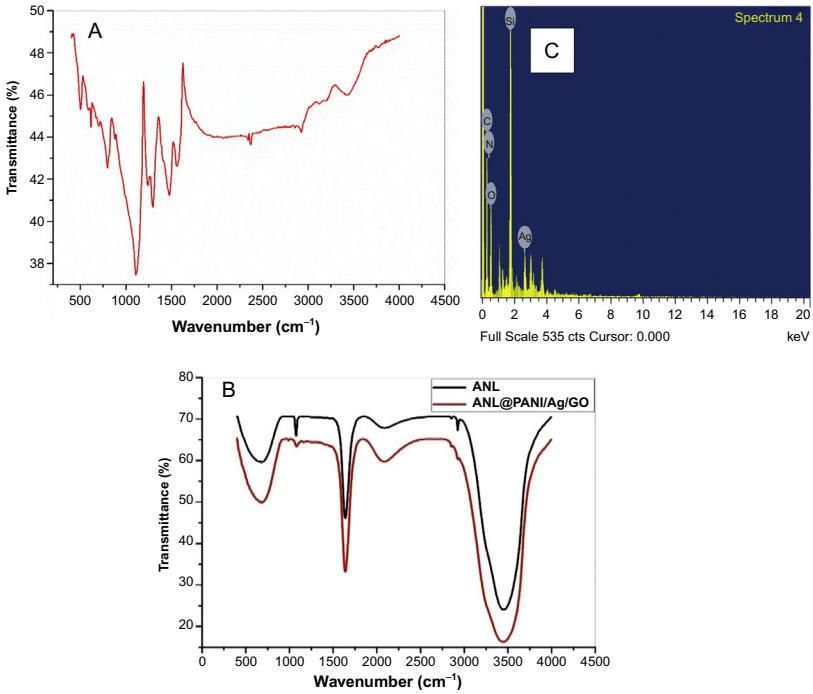

Fig. 12 FT-IR analysis is performed to monitor the linkages present between lipase and PANI/Ag/GONC. FT-IR spectra of (A) PANI/Ag/GONC, (B) ANL and ANL@PANI/Ag/GONC, these measurements were carried out on Perkin Elmer FT-IR spectrometer, Spectrum Two (CT, USA), and (C) EDAX analysis. *Reproduced from Asmat, S., Husain, Q., & Azam, A. (2017). Lipase immobilization on facile synthesized polyaniline-coated silver-functionalized graphene oxide nanocomposites as novel biocatalysts: stability and activity insights.* RSC Advances, *7(9), 5019–5029.*

examine the presence of characteristic functional groups of NC before and after immobilization and the changes occurring in them. Fig. 12 represents the spectra of synthesized NC, free ANL, and ANL@PANI/Ag/GONC. The FT-IR spectra of NC displays peak in the wavenumber range 1085, 1440, 1580, and 3425 cm^{-1} which indicate C—O bonds, C—N stretching vibration of slightly reduced Ag–GO, C═C bonds and oxygenated functional groups –OH, respectively (Chen, Feng, & Li, 2012). The FT-IR spectrum of ANL revealed dominant signals in the wavenumber range 3420–3150 cm^{-1} (–OH stretching vibrations and –NH stretching vibrations), at 2924 cm^{-1} (C—H stretching vibrations), 1652 cm^{-1} (N—H bending vibrations) whose intensity was considerably increased after binding with PANI/Ag/GONC, clearly signifying the successful immobilization of the enzyme onto NC (Hou, Qi, & Zhu, 2015). EDAX mapping examines

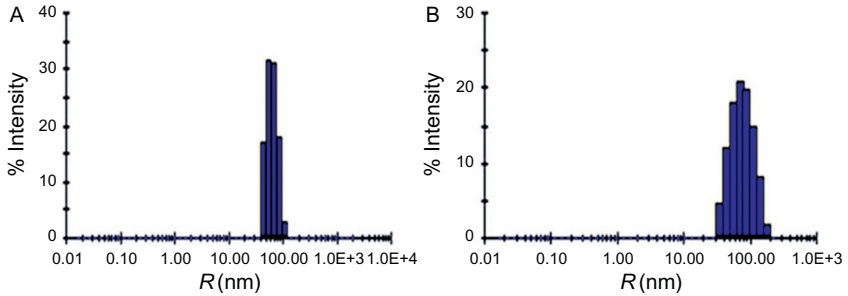

Fig. 13 DLS measurements showing hydrodynamic size distribution of (A) PANI/Ag/GONC and (B) ANL@PANI/Ag/GONC. *Reproduced from Asmat, S., Husain, Q., & Azam, A. (2017). Lipase immobilization on facile synthesized polyaniline-coated silver-functionalized graphene oxide nanocomposites as novel biocatalysts: stability and activity insights.* RSC Advances, *7(9), 5019–5029.*

the elemental distribution and structure of the NC (Rezaei, Akhavan, Hashemi, & Shamsara, 2016). The outcome can be seen in Fig. 12 in which the characteristic peaks of C, Ag, O, N_2, and Si are visible, with Gr designated through C peaks. The NC was visualized on the silica cover slip and thus the corresponding peak for Si was visible.

DLS is a technique which is used to analyze the size distribution profile of particles in solutions or suspension which provides us information regarding the conjugation of enzyme with NM (Venditti et al., 2015). Herein, it was employed to inspect the size and polydispersity of PANI/Ag/GONC and ANL@PANI/Ag/GONC. As shown in Fig. 13, the hydrodynamic radii (Rh) and percent polydispersity of free NCs were 62 nm and 24.5%, respectively. These values increased remarkably after binding with ANL. The Rh and percent polydispersity values were 100 nm and 32.6%, after immobilization, respectively, and this might be possibly due to aggregation of bigger particles with smaller ones.

3.9 Immobilization Efficiency of ANL@PANI/Ag/GONC

Glutaraldehyde has been used as a crosslinker to immobilize ANL on PANI/Ag/GONC, which was achieved by covalent attachment as displayed in the schematic representation of the formulation of ANL@PANI/Ag/GONC (Fig. 14). The immobilized lipase formulation showed an effectiveness factor (η) of 0.94. The η value of an immobilized enzyme preparation represents the ratio of actual to theoretical activity of the immobilized enzyme preparation (Matto, Naqash, & Husain, 2008). Table 6 displays the immobilization efficiency of bound lipase.

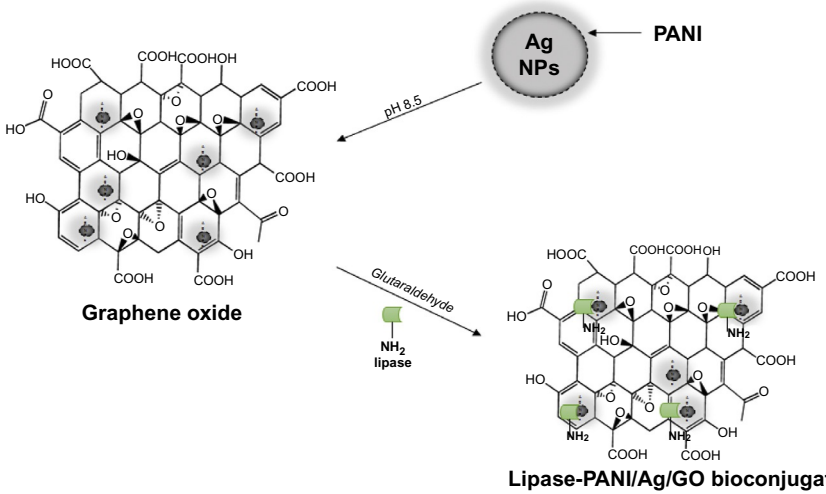

Fig. 14 Schematic illustration of preparation of ANL@PANI/Ag/GONC. *Reproduced from Asmat, S., Husain, Q., & Azam, A. (2017). Lipase immobilization on facile synthesized polyaniline-coated silver-functionalized graphene oxide nanocomposites as novel biocatalysts: stability and activity insights.* RSC Advances, *7(9), 5019–5029.*

Table 6 Immobilization of Lipase on PANI/Ag/GONC

		Enzyme Activity Bound to PANI/Ag/GONC			
Enzyme Loaded (*X*) (U)	**Enzyme Activity in Washes (*Y*) (U)**	**Theoretical (*X* − *Y*) = (*A*)**	**Actual (*B*)**	**Effectiveness Factor (η) = (*B*/*A*)**	**Immobilization Yield (%) (*B*/*A* × 100)**
7	0.4	6.6	6.2	0.94	94

Each value demonstrates the mean for three independent experiments performed in triplicates.
Reproduced from Asmat, S., Husain, Q., & Azam, A. (2017). Lipase immobilization on facile synthesized polyaniline-coated silver-functionalized graphene oxide nanocomposites as novel biocatalysts: stability and activity insights. *RSC Advances*, 7(9), 5019–5029.

3.10 Stability Studies of ANL@PANI/Ag/GONC

Fig. 15A demonstrates the biocatalytic activity of free and PANI/Ag/GONC bound ANL at various temperatures and in buffers of various pH values. The free ANL showed its temperature optima at 40°C, whereas the fabricated nanobiocatalyst exhibited its temperature optima at 45°C. The immobilized ANL retained over 90% of its initial activity from 35 to 50°C demonstrating that ANL@PANI/Ag/GONC was more resistant

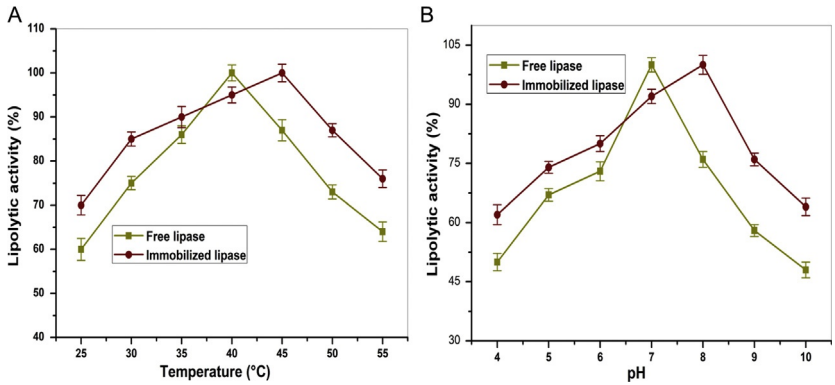

Fig. 15 (A) Temperature–activity profiles for free and immobilized lipase. The activity obtained at 40°C was taken as reference (100%) for the calculation of remaining percent activity. (B) Optimal pH–activity profiles for free and immobilized lipase. The activity at pH 7 was taken as control (100%) for the determination of remaining percent activity. The *symbols* show (–■–) free and (–●–) immobilized lipase. *Reproduced from Asmat, S., Husain, Q., & Azam, A. (2017). Lipase immobilization on facile synthesized polyaniline-coated silver-functionalized graphene oxide nanocomposites as novel biocatalysts: stability and activity insights.* RSC Advances, *7(9), 5019–5029.*

against heat as compared to free ANL (Hou et al., 2015). ANL and ANL@PANI/Ag/GONC exhibited their maximum activity at pH 7.0 and 8.0, respectively. However, ANL@PANI/Ag/GONC showed an increased resistance in a pH range from 7.0 to 9.0. ANL@PANI/Ag/GO retained higher fractions of catalytic activity in alkaline region as compared to free ANL. It might be due to electrostatic interactions and hydrogen bonding between ANL and the nanosupport (Suplatov et al., 2014).

Fig. 16A depicts the storage stability for free and PANI/Ag/GONC bound ANL, where both preparations have been incubated at temperatures 4 and 30°C. The results showed that the constructed nanobiocatalyst retained significantly higher activity when stored at both temperatures. ANL@PANI/Ag/GONC maintained 88% of its original activity after 30 days of storage at 4°C, whereas free enzyme showed about 65% of the initial activity under similar storage conditions. The decrease in the catalytic activity could be due to conformational changes in ANL, which can be improved upon immobilization as it provides rigidity to the enzyme (Yang et al., 2016).

Fig. 16B presents the thermal stability analysis for free and immobilized ANL. The free enzyme lost 51% of its activity after 2 h incubation at 60°C, while fabricated nanobioconjugate retained 85% activity under similar

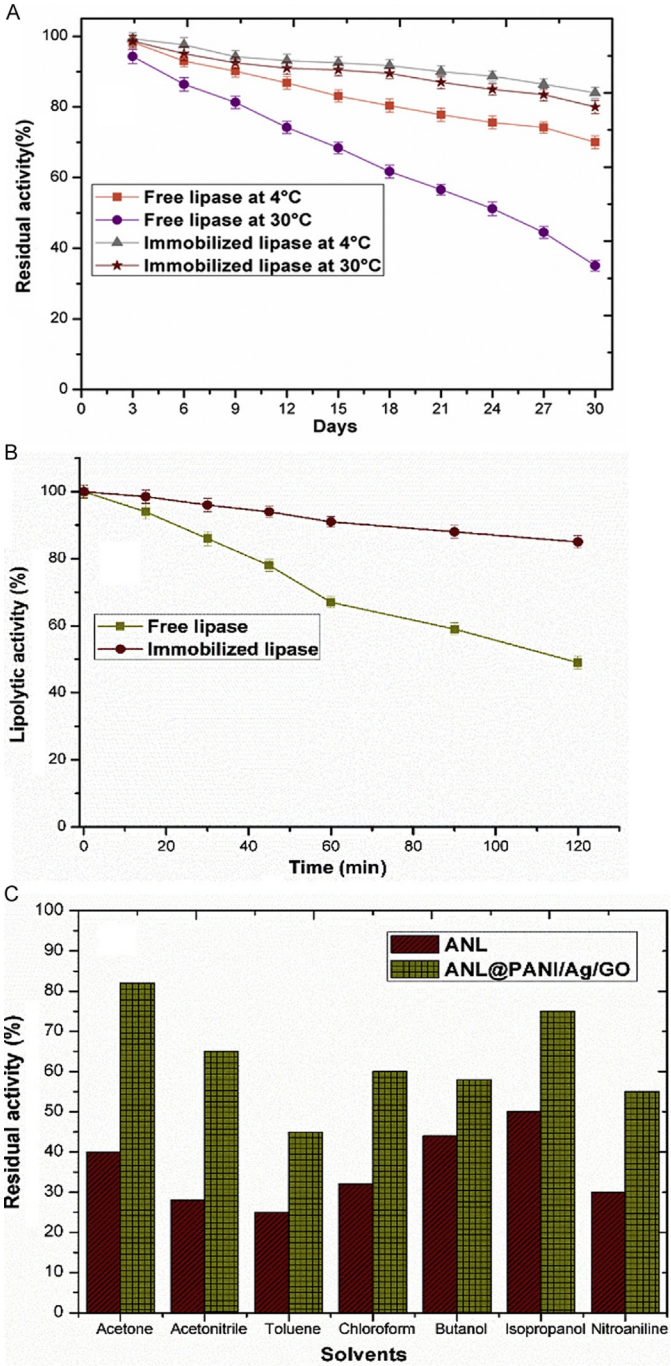

Fig. 16 Stability of free and PANI/Ag/GONC bound ANL. (A) Storage stability at 4°C and 30°C; (B) thermal denaturation; and (C) solvent stability. *Reproduced from Asmat, S., Husain, Q., & Azam, A. (2017). Lipase immobilization on facile synthesized polyaniline-coated silver-functionalized graphene oxide nanocomposites as novel biocatalysts: stability and activity insights.* RSC Advances, *7(9), 5019–5029.*

conditions. ANL@PANI/Ag/GONC showed better solvent tolerance as compared to its free enzyme in the presence of seven investigated solvents (Fig. 16C). Isopropanol exhibited lowest toxicity to free ANL, while acetone displayed lowest toxicity to ANL@PANI/Ag/GONC as its residual activity was high (81.5%). Likewise, 1 h incubation with toluene caused nearly 75% loss of activity in free ANL, but ANL@PANI/Ag/GONC maintained 55% of its original activity during similar exposure. We have recently reported similar enhancement in enzyme activity by solvent exposure (Asmat, Husain, & Khan, 2018). The prepared lipase@Ppy-MA/TiO_2-NC preparation displayed remarkable improved activity against solvent tolerance (150% and 125% activity recovery in acetone and isopropanol) as compared to its free counterpart. Usually, upon contact with organic solvents or ionic liquids, stripping of water from the protein surface is seen, in addition to solvent penetration into the enzyme, causing the protein to unfold and in turn, deactivation of the enzyme results (Romero et al., 2012). However, it has been observed that after the immobilization of lipase on PANI/Ag/GONC, organic solvents do not simply strip off the aqueous layer from the protein surface, thereby sustaining catalytic conformation and inner rigidity of the enzyme.

3.11 Reusability Analysis of ANL@PANI/Ag/GONC

Enzyme recovery provides a number of cost advantages that are often an essential prerequisite for establishing an economically viable enzyme catalyzed process. ANL@PANI/Ag/GONC maintained nearly 85% activity after its 11th repeated use (Fig. 17). There was a slight loss in its catalytic activity that might be during centrifugation after each repeated use. The PANI/Ag/GONC bound lipase retained significantly high catalytic activity even after its 11th repeated use, thereby enhancing its industrial applicability.

4. SUMMARY AND FUTURE OUTLOOK

Gr-based NM have rapidly become the most widely studied carbon-based materials owing to their unique structural features and exceptionally high chemical, electrical, and mechanical properties, as well as their capability for multivalent functionalization and efficient loading of biomacromolecules. The remarkable progress in synthesis and surface engineering of Gr-NM has opened new avenues exploring their use as nanoscaffolds for the development of nanobiocatalytic systems. These novel

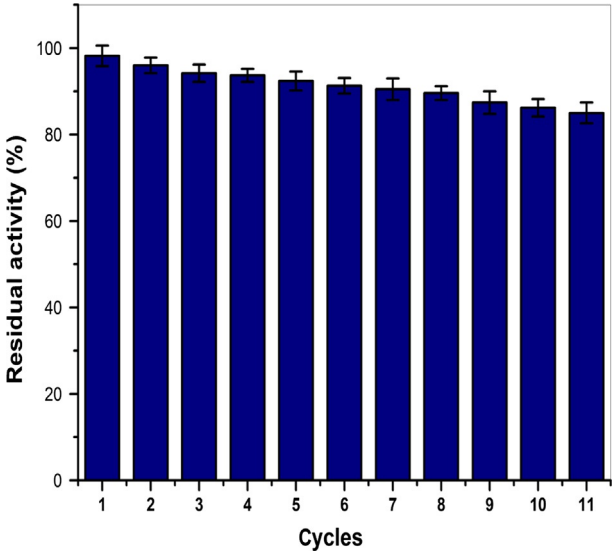

Fig. 17 Reusability assay of ANL@PANI/Ag/GONC. The enzyme activity calculated on the first day was taken as the reference (100%) for the determination of the remaining percentage activity after each reuse. *Reproduced from Asmat, S., Husain, Q., & Azam, A. (2017). Lipase immobilization on facile synthesized polyaniline-coated silver-functionalized graphene oxide nanocomposites as novel biocatalysts: stability and activity insights.* RSC Advances, *7(9), 5019–5029.*

bioconjugates differ from traditional immobilized enzymes in terms of catalytic efficiency, operational stability, and application potential.

In this chapter, an effort has been made to describe techniques employed in the synthesis and characterization of Gr-NC. The Gr-NC has been further used to immobilize industrially important hydrolytic enzymes; β-galactosidase and lipase. Two different approaches for the production of Gr-armored proteins have been discussed here. The first approach involved the physical adsorption of β-galactosidase on Gr@Fe_3O_4 NC, while the other made the use of glutaraldehyde, a crosslinking agent to covalently bind lipase with ANL@PANI/Ag/GONC.

In the first study, efficient immobilization of *A. oryzae* β-galactosidase onto functionalized Gr sheets (Gr@Fe_3O_4 NC) has been investigated. This support was selected because it provided high stability to enzyme and it is also nontoxic in nature. The immobilized β-galactosidase exhibited remarkably high storage stability and was found less inhibitory to its own product galactose as compared to its free form. Furthermore, this fabricated biocatalyst may be simply separated from the reaction mixture by magnetization or

low speed centrifugation, and exhibited excellent reusability over several successive repeated uses. Hence, such robust nanobiocatalyst can serve as a powerful biorecognition probe for biosensor applications. One can detect the lactose concentrations in milk easily and efficiently by applying the biosensor armored with the help of such type of material. Utility of this method can be further extended in the development of therapeutic agents for targeted drug delivery for lactose intolerant patients.

In the second investigation of this chapter, a polymer modified silver incorporated GO NC (ANL@PANI/Ag/GONC) has been fabricated and used to immobilize enzyme lipase from *A. niger*. Lipase armored to this GO NC appeared significantly more stable to various kinds of denaturants, particularly it was noticed that PANI/Ag/GONC bound enzyme exhibited high resistance to denaturation mediated by various organic solvents. The immobilized enzyme can be applied for catalysis of some novel reactions such as acylation, esterification, transesterification, and interesterification.

The methods employed in the earlier studies have advantages as well as drawbacks. Enzyme leaching, which is a major problem associated with noncovalent immobilization techniques can be significantly reduced by crosslinking the enzyme with glutaraldehyde, which subsequently provides multipoint attachment of enzyme with the support. As can be inferred from the earlier investigations, in the second approach involving covalent method of binding, immobilized lipase retained 94% activity as compared to physically adsorbed β-galactosidase which was able to maintain 89% activity. Similarly, when the reusability was assessed, the immobilized lipase preparation exhibited 85% enzyme activity even after its 11 reuses, whereas the immobilized β-galactosidase was able to retain about 80% of the activity after its ninth cycle of repetitive use. Although the progress in the field is very promising, some critical points still need to be addressed in order to expand the applications of Gr-NC as immobilization matrices in nanobiotechnology. Further investigation is required to gain a deeper understanding of the effects of Gr-NC on the structure and functions of enzymes and other proteins. For instance, studying the effect of the type of functionalization as well as the structure and physicochemical characteristics of engineered Gr-NM on the immobilization efficiency and orientation of proteins will provide further understanding of the interactions of NM with protein molecules, which could lead to optimization of nanobiocatalytic systems.

Extensive characterization of enzymes and armored nanosupport would allow a better understanding of the role of binding moieties involved in the

immobilization process and this would further help in scaling up these nanobiocatalysts in a cost effective and an efficient manner. For example, circular dichroism and 3D spectroscopic studies can be conducted to reveal the conformational changes in the immobilized protein with regard to protein-structure and function, which would broaden our knowledge on such fascinating nanobiocatalytic materials. Furthermore, an added focus would be to develop efficient Gr-NC with high biocompatibility, reduced toxicity, and negligible environmental effect, is essential for creating assemblies and functional devices that will expand the applications of Gr-NC in the field of biocatalytic transformations, enzyme engineering, biofuel and energy production, enzyme-based biosensing, and bioassays. Systematic comparisons of the performance of different kinds of Gr-NC is needed to establish a principle for the application of Gr-related NM in biosensors and other fields. Compared with carbon nanotubes (CNTs), limited research has been carried out on Gr/conducting polymer NC and Gr/carbon paste electrodes. Finally, the mass production of single-layer Gr is a major challenge that, if overcome, could benefit. In any case, the future of Gr is indeed bright.

ACKNOWLEDGMENTS

USIF, AMU, is duly acknowledged for providing the facilities of TEM and SEM. VSM and FT-Raman technique were performed in SAIF, IIT, Madras, while AFM was conducted at IIT Kanpur instrumentation facility. Centre of Excellence in Materials Science (Nanomaterials), Department of Applied Physics, Z.H. College of Engineering & Technology, AMU is duly acknowledged for providing TGA.

FUNDING

M.K. gratefully acknowledges the financial assistance in terms of "SRF" by "UGC-MANF, New Delhi." We are also grateful for funding support by UGC in terms of "University Non-NET fellowship" to one of our coauthors, S.M.

REFERENCES

Allen, M. J., Tung, V. C., & Kaner, R. B. (2010). Honeycomb carbon: A review of graphene. *Chemical Reviews*, *110*, 132–145.

Al-Lolage, F. A., Meneghello, M., Ma, S., Ludwig, R., & Bartlett, P. N. (2017). A flexible method for the stable, covalent immobilization of enzymes at electrode surfaces. *ChemElectroChem*, *4*, 1528–1534.

Alsharaeh, E. H., Othman, A. A., & Aldosari, M. A. (2014). Microwave irradiation effect on the dispersion and thermal stability of RGO nanosheets within a polystyrene matrix. *Materials (Basel, Switzerland)*, 7, 5212–5224.

Amirbandeh, M., & Taheri-Kafrani, A. (2016). Immobilization of glucoamylase on triazine-functionalized Fe_3O_4/graphene oxide nanocomposite: Improved stability and reusability. *International Journal of Biological Macromolecules*, *93*, 1183–1191.

Ansari, S. A., & Husain, Q. (2010). Lactose hydrolysis by β galactosidase immobilized on concanavalin A-cellulose in batch and continuous mode. *Journal of Molecular Catalysis B: Enzymatic*, *63*, 68–74.

Ansari, S. A., & Husain, Q. (2011a). Immobilization of *Aspergillus oryzae* 456 ß-galactosidase on concanavalin A-layered calcium alginate-cellulose beads and its application in lactose hydrolysis in continuous spiral bed reactors. *Polish Journal of Chemical Technology*, *13*, 15–20.

Ansari, S. A., & Husain, Q. (2011b). Immobilization of *Kluyveromyces lactis* β galactosidase on concanavalin A layered aluminium oxide nanoparticles—Its future aspects in biosensor applications. *Journal of Molecular Catalysis B: Enzymatic*, *70*, 119–126.

Ansari, S. A., & Husain, Q. (2012). Potential applications of enzymes immobilized on/in nano materials: A review. *Biotechnology Advances*, *30*, 512–523.

Apetrei, I. M., & Apetrei, C. (2016). Amperometric biosensor based on diamine oxidase/platinum nanoparticles/graphene/chitosan modified screen-printed carbon electrode for histamine detection. *Sensors*, *16*, 422–429.

Asmat, S., Husain, Q., & Khan, M. S. (2018). A polypyrrole–methyl anthranilate functionalized worm-like titanium dioxide nanocomposite as an innovative tool for immobilization of lipase: Preparation, activity, stability and molecular docking investigations. *New Journal of Chemistry*, *42*, 91–102.

Baby, T. T., Aravind, S. S. J., Arockiadoss, T., Rakhi, R. B., & Ramaprabhu, S. (2010). Metal decorated graphene nanosheets as immobilization matrix for amprometric biosensor. *Sensors and Actuators B: Chemical*, *145*, 71–77.

Bao, H., Chen, Q., Zhang, L., & Chen, G. (2011). Immobilization of trypsin in the layer-by-layer coating of graphene oxide and chitosan on in-channel glass fiber for microfluidic proteolysis. *Analyst*, *136*, 5190–5196.

Bao, H., Zhang, L., & Chen, G. (2013). Immobilization of trypsin via graphene oxide-silica composite for efficient microchip proteolysis. *Journal of Chromatography*, *1310*, 74–81.

Bathinapatla, A., Kanchi, S., Singh, P., Sabela, M. I., & Bisetty, K. (2016). An ultrasensitive performance enhanced novel cytochrome c biosensor for the detection of rebaudioside A. *Biosensors & Bioelectronics*, *77*, 116–123.

Bayraktar, H., Serilmiz, M., Karakas, T. E., Celem, B., & Onal, S. (2011). Immobilization and stabilization of α-galactosidase on Sepabeads EC-EA and EC-HA. *International Journal of Biological Macromolecules*, *49*, 855–860.

Cao, Y., Wen, L., Svec, F., Tan, T., & Lv, Y. (2016). Magnetic AuNP@ Fe_3O_4 nanoparticles as reusable carriers for reversible enzyme immobilization. *Chemical Engineering Journal*, *286*, 272–281.

Chandra, V., Park, J., Chun, Y., Lee, J. W., Hwang, I. C., & Kim, K. S. (2010). Water dispersible magnetite-reduced graphene oxide composites for arsenic removal. *ACS Nano*, *4*, 3979–3986.

Chang, Q., Huang, J., Ding, Y., & Tang, H. (2016). Catalytic oxidation of phenol and 2,4-dichlorophenol by using horseradish peroxidase immobilized on graphene oxide/Fe_3O_4. *Molecules*, *21*, 1044–1051.

Chang, Q., Jiang, G., Tang, H., Li, N., Huang, J., & Wu, L. (2015). Enzymatic removal of chlorophenols using horseradish peroxidase immobilized on superparamagnetic Fe_3O_4/graphene oxide nanocomposites. *Chinese Journal of Catalysis*, *36*, 961–968.

Chauhan, N., Chawla, S., Pundir, C. S., & Jain, U. (2017). An electrochemical sensor for detection of neurotransmitter-acetylcholine using metal nanoparticles, 2D material and conducting polymer modified electrode. *Biosensors & Bioelectronics*, *89*, 377–383.

Chen, D., Feng, H., & Li, J. (2012). Graphene oxide: Preparation, functionalization, and electrochemical applications. *Chemical Reviews*, *112*, 6027–6053.

Chen, J., Leng, J., Yang, X., Liao, L., Liu, L., & Xiao, A. (2017). Enhanced performance of magnetic graphene oxide-immobilized laccase and its application for the decolorization of dyes. *Molecules*, *22*, 221–230.

Chen, D., Tang, L., & Li, J. (2010). Graphene-based materials in electrochemistry. *Chemical Society Reviews*, *39*, 3157–3180.

Cho, Y., Kim, H., & Choi, Y. (2013). A graphene oxide-photosensitizer complex as an enzyme-activatable theranostic agent. *Chemical Communications*, *49*, 1202–1204.

Choi, B. G., Park, H., Yang, M. H., Jung, Y. M., Lee, S. Y., Hong, W. H., et al. (2010). Microwave-assisted synthesis of highly water-soluble graphene towards electrical DNA sensor. *Nanoscale*, *2*, 2692–2697.

Dai, L. (2013). Functionalization of graphene for efficient energy conversion and storage. *Accounts of Chemical Research*, *46*, 31–42.

Das, R., Talat, M., Srivastava, O. N., & Kayastha, A. M. (2018). Covalent immobilization of peanut β-amylase for producing industrial nano-biocatalysts: A comparative study of kinetics, stability and reusability of the immobilized enzyme. *Food Chemistry*, *245*, 488–499.

Das, G., & Yoon, H. H. (2015). Amperometric urea biosensors based on sulfonated graphene/polyaniline nanocomposite. *International Journal of Nanomedicine*, *10*, 55–66.

Dutta, N., Biswas, S., & Saha, M. K. (2016). Biophysical characterization and activity analysis of nano-magnesium supplemented cellulase obtained from a psychrobacterium following graphene oxide immobilization. *Enzyme and Microbial Technology*, *95*, 248–258.

Dutta, A., Biswas, S., & Saha, M. K. (2017). Nano-magnesium aided activity enhancement and biophysical characterization of a psychrophilic α-amylase immobilized on graphene oxide nanosupport. *Journal of Bioscience and Bioengineering*, *124*, 15–22.

Eigler, S. M., Dotzer, C., & Hirsch, A. (2012). Formation and decomposition of CO_2 intercalated graphene oxide. *Carbon*, *50*, 3666–3673.

EzhiVilian, E. T., Giribabu, K., Choe, S. R., Muruganantham, R., Lee, H., Roh, C., et al. (2017). A spick-and-span approach to the immobilization of horseradish peroxidase on Au nanospheres incorporated with a methionine/graphene biomatrix for the determination of endocrine disruptor bisphenol A. *Sensors and Actuators B: Chemical*, *251*, 804–812.

Fartas, F. M., Abdullah, J., Yusof, N. A., Sulaiman, Y., & Saiman, M. I. (2017). Biosensor based on tyrosinase immobilized on graphene-decorated gold nanoparticle/chitosan for phenolic detection in aqueous. *Sensors*, *17*, 1132–1139.

Feng, L. Y., Wu, L., & Qu, X. G. (2013). New horizons for diagnostics and therapeutic applications of graphene and graphene oxide. *Advanced Materials*, *25*, 168–186.

Gao, L., Zhang, H., & Cui, H. (2014). A general strategy to prepare homogeneous and reagentless GO/lucigenin & enzyme biosensors for detection of small biomolecules. *Biosensors & Bioelectronics*, *57*, 65–70.

Ge, J., Yang, C., Zhu, J., Lu, D., & Liu, Z. (2012). Nanobiocatalysis in organic media: Opportunities for enzymes in nanostructures. *Topics in Catalysis*, *55*, 1070–1080.

Geim, A. K., & Novoselov, K. S. (2007). The rise of graphene. *Nature Materials*, *6*, 183–191.

Georgakilas, V. (2012). Functionalization of graphene: Covalent and non-covalent approaches, derivatives and applications. *Chemical Reviews*, *112*, 6156–6214.

Goenka, S., Sant, V., & Sant, S. (2014). Graphene-based nanomaterials for drug delivery and tissue engineering. *Journal of Controlled Release*, *173*, 75–88.

Gokhale, A. A., Lu, J., & Lee, I. (2013). Immobilization of cellulase on magnetoresponsive graphene nano-supports. *Journal of Molecular Catalysis B: Enzymatic*, *90*, 76–86.

Gomes, A. A., Telli, E. P., Miletti, L. C., Skoronski, E., Ghislandi, M. G., Da Silva, G. F., et al. (2017). Improved enzymatic performance of graphene-immobilized β-glucosidase A in the presence of glucose-6-phosphate. *Biotechnology and Applied Biochemistry*, *15*, 1569–1574.

Haider, T., & Husain, Q. (2007). Calcium alginate entrapped preparations of *Aspergillus oryzae* β galactosidase: Its stability and applications in the hydrolysis of lactose. *International Journal of Biological Macromolecules*, *41*, 72–80.

Halder, A., Zhang, M., & Chi, Q. (2017). Electroactive and biocompatible functionalization of graphene for the development of biosensing platforms. *Biosensors & Bioelectronics*, *87*, 764–771.

He, H., & Gao, C. (2010). Supraparamagnetic, conductive, and processable multifunctional graphene nanosheets coated with high-density Fe_3O_4 nanoparticles. *ACS Applied Materials & Interfaces*, *2*, 3201–3210.

He, L. H., Zhang, Y. C., Liu, S. L., Fang, S. M., & Zhang, Z. H. (2014). A nanocomposite consisting of plasma-polymerized propargylamine and graphene for use in DNA sensing. *Microchimica Acta*, *181*, 1981–1989.

Heldt, C. L., Sieloff, A. K., Merillat, J. P., Minerick, A. R., King, J. A., Perger, W. F., et al. (2013). Stacked graphene nanoplatelet paper sensor for protein detection. *Sensors and Actuators B: Chemical*, *181*, 92–98.

Hernaez, M., Zammareno, C. R., Melendi-Espina, S., Bird, L. R., Mayes, A. G., & Arregui, F. J. (2017). Optical fibre sensors using graphene-based materials: A review. *Sensors*, *17*, 155.

Hossain, M. F., & Park, J. Y. (2017). Fabrication of sensitive enzymatic biosensor based on multi-layered reduced graphene oxide added PtAu nanoparticles-modified hybrid electrode. *PLoS One*, *12*, 173553.

Hou, C., Qi, Z., & Zhu, H. (2015). Preparation of core–shell magnetic polydopamine/alginate biocomposite for *Candida rugosa* lipase immobilization. *Colloids and Surfaces B: Biointerfaces*, *128*, 544–551.

Husain, Q. (2010). β-Galactosidases and their potential applications: A review. *Critical Reviews in Biotechnology*, *30*, 41–62.

Husain, Q. (2016). Magnetic nanoparticles as a tool for the immobilization/stabilization of hydrolases and their applications: An overview. *Biointerface Research in Applied Chemistry*, *6*, 1585–1606.

Husain, Q. (2017a). Nanomaterials as novel support for the immobilization of amylolytic enzymes and their application: A review. *Biocatalysis*, *3*, 31–53.

Husain, Q. (2017b). Nanomaterials immobilized cellulolytic enzymes and their industrial applications: A literature review. *JSM Biochemistry and Molecular Biology*, *4*, 1029–1045.

Husain, Q. (2017c). Nanosupport bound lipases, their stability and applications. *Biointerface Research in Applied Chemistry*, *7*, 2194–2216.

Husain, Q. (2017d). High yield immobilization and stabilization of oxidoreductases using magnetic nanosupports and their potential applications: An update. *Current Catalysis*, *6*, 168–187.

Husain, Q. (2017e). Biosensor applications of graphene-nanocomposites bound oxidoreductive and hydrolytic enzymes. *Analytical Methods*, *9*, 6734–6746.

Husain, Q. (2018a). Nanocarriers immobilized proteases and their industrial applications: An overview. *Journal of Nanoscience and Nanotechnology*, *18*, 486–499.

Husain, Q. (2018b). Carbon nanotubes mediated immobilized glucose oxidase biosensors as an effective and sensitive analytical tool. *Biointerface Research in Applied Chemistry*, *8*, 3060–3074.

Husain, Q., Ansari, S. A., Alam, F., & Azam, A. (2011). Immobilization of *Aspergillus oryzae* β galactosidase on zinc oxide nanoparticles via simple adsorption mechanism. *International Journal of Biological Macromolecules*, *49*, 37–43.

Husain, Q., & Qayyum, S. (2013). Biological and enzymatic treatment of bisphenol A and other endocrine disrupting compounds: A review. *Critical Reviews in Biotechnology*, *33*, 260–292.

Husain, Q., & Ulber, R. (2011). Immobilized peroxidase as a valuable tool in the remediation of aromatic pollutants and xenobiotic compounds: A review. *Critical Reviews in Environmental Science and Technology*, *41*, 770–804.

Hwa, K. Y., & Subramani, B. (2014). Synthesis of zinc oxide nanoparticles on graphene–carbon nanotube hybrid for glucose biosensor applications. *Biosensors & Bioelectronics*, *62*, 127–133.

Jiang, D., Liu, Q., Wang, K., Qian, J., Dong, X., Yang, Z., et al. (2014). Enhanced non-enzymatic glucose sensing based on copper nanoparticles decorated nitrogen-doped graphene. *Biosensors & Bioelectronics*, *54*, 273–278.

Jiang, B., Yang, K., Zhang, L., Liang, Z., Peng, X., & Zhang, Y. (2014). Dendrimer-grafted graphene oxide nanosheets as novel support for trypsin immobilization to achieve fast on-plate digestion of proteins. *Talanta*, *122*, 278–284.

Jiang, B., Yang, K., Zhao, Q., Wu, Q., Liang, Z., Zhang, L., et al. (2012). Hydrophilic immobilized trypsin reactor with magnetic graphene oxide as support for high efficient proteome digestion. *Journal of Chromatography A*, *1254*, 8–13.

Johnson, P. A., Park, H. J., & Driscoll, A. J. (2011). Enzyme nanoparticle fabrication: Magnetic nanoparticle synthesis and enzyme immobilization. *Methods in Molecular Biology*, *679*, 183–191.

Khan, M. J., Husain, Q., & Ansari, S. A. (2013). Polyaniline-assisted silver nanoparticles: A novel support for the immobilization of α-amylase. *Applied Microbiology and Biotechnology*, *97*, 1513–1522.

Khan, M., Husain, Q., & Naqvi, A. H. (2016). Graphene based magnetic nanocomposites as versatile carriers for high yield immobilization and stabilization of β-galactosidase. *RSC Advances*, *6*, 53493–53503.

Khan, M. J., Qayyum, S., Alam, F., & Husain, Q. (2011). Effect of tin oxide nanoparticle binding on the structure and activity of α-amylase from *Bacillus amyloliquefaciens*. *Nanotechnology*, *22*, 455708.

Krishna, K. V., Menard-Moyon, C., Verma, S., & Bianco, A. (2013). Graphene-based nanomaterials for nanobiotechnology and biomedical applications. *Nanomedicine*, *8*, 1669–1688.

Kuila, T., Bose, S., Khanra, P., Mishra, A. K., Kim, N. H., & Lee, J. H. (2011). Recent advances in graphene-based biosensors. *Biosensors & Bioelectronics*, *26*, 4637–4678.

Kurbanoglu, S., Rivas, L., Ozkan, S. A., & Merkoçi, A. (2017). Electrochemically reduced graphene and iridium oxide nanoparticles for inhibition-based angiotensin-converting enzyme inhibitor detection. *Biosensors & Bioelectronics*, *88*, 122–129.

Li, M., Yang, X., Ren, J., Qu, K., & Qu, X. (2012). Using graphene oxide high near-infrared absorbance for photothermal treatment of Alzheimer's disease. *Advanced Materials*, *24*, 1722–1728.

Liang, R. P., Wang, X. N., Liu, C. M., Meng, X. Y., & Qiu, J. D. (2013). Construction of graphene oxide magnetic nanocomposites-based on-chip enzymatic microreactor for ultrasensitive pesticide detection. *Journal of Chromatography A*, *1315*, 28–35.

Lin, Y. C., Lu, C. C., Yeh, C. H., Jin, C., Suenaga, K., & Chiu, P. W. (2012). Graphene annealing: How clean can it be? *Nano Letters*, *12*, 414–419.

Liu, N., & Ma, Z. F. (2014). Au-ionic liquid functionalized reduced graphene oxide immunosensing platform for simultaneous electrochemical detection of multiple analytes. *Biosensors & Bioelectronics*, *51*, 184–190.

Liu, Y. P., Yuan, L., Yang, M., Zheng, Y., Li, L. J., Gao, L., et al. (2014). Giant enhancement in vertical conductivity of stacked CVD graphene sheets by self-assembled molecular layers. *Nature Communications*, *20*, 5461.

Liu, X., Zhang, J., Yan, R., Zhang, Q., & Liu, X. (2014). Preparation of graphene nanoplatelet-titanate nanotube composite and its advantages over the two single components as biosensor immobilization materials. *Biosensors & Bioelectronics*, *51*, 76–81.

Loh, K. P., Bao, Q., Ang, P. K., & Yang, J. (2010). The chemistry of graphene. *Journal of Materials Chemistry*, *20*, 2277–2289.

Mahdevi, M., Ahmad, M. B., Haron, M. J., Namvar, F., Nadi, B., Rahman, M. Z. A., et al. (2013). Synthesis, surface modification and characterization of biocompatible magnetic iron oxide nanoparticles for biomedical applications. *Molecules*, *18*, 7533–7548.

Mansouri, N., Babadi, A. A., Bagheri, S., & Abd Hamid, S. B. (2017). Immobilization of glucose oxidase on 3D graphene thin film: Novel glucose bioanalytical sensing platform. *International Journal of Hydrogen Energy*, *42*, 1337–1343.

Mateo, C., Palomo, J. M., Lorente, G. F., Guisan, J. M., & Lafuente, R. F. (2007). Improvement of enzyme activity, stability and selectivity via immobilization techniques. *Enzyme Microbial Technology*, *40*, 1451–1463.

Matto, M., Naqash, S., & Husain, Q. (2008). An economical and simple bioaffinity support for the immobilization and stabilization of tomato (Lycopersicon esculentum) peroxidase. *Acta Chimica Slovenica*, *55*, 671–676.

Narayanan, T. N., Liu, Z., Lakshmy, P., Gao, P., Nagoka, Y., Kumar, D. S., et al. (2012). Synthesis of reduced graphene oxide–Fe_3O_4 multifunctional freestanding membranes and their temperature dependent electronic transport properties. *Carbon*, *50*, 1338–1345.

Novoselov, K. S., Geim, A. K., & Morozov, S. V. (2004). Electric field effect in atomically thin carbon films. *Science*, *306*, 666–669.

Ormategui, N., Veloso, A., Leal, G. P., Rodriguez-Couto, S., & Tomovska, R. (2015). Design of stable and powerful nanobiocatalysts, based on enzyme laccase immobilized on self-assembled 3D graphene/polymer composite hydrogels. *ACS Applied Materials & Interfaces*, *7*, 14104–14112.

Pakapongpan, S., & Poo-Arporn, R. P. (2017). Self-assembly of glucose oxidase on reduced graphene oxide-magnetic nanoparticles nanocomposite-based direct electrochemistry for reagentless glucose biosensor. *Materials Science & Engineering C: Materials for Biological Applications*, *76*, 398–405.

Palanisamy, S., Cheemalapati, S., & Chen, S. M. (2014). Amperometric glucose biosensor based on glucose oxidase dispersed in multiwalled carbon nanotubes/graphene oxide hybrid biocomposite. *Materials Science and Engineering C: Materials for Biology Applications*, *34*, 207–213.

Palanisamy, S., Karuppiah, C., & Chen, S. M. (2014). Direct electrochemistry and electrocatalysis of glucose oxidase immobilized on reduced graphene oxide and silver nanoparticles nanocomposite modified electrode. *Colloids and Surfaces B: Biointerfaces*, *114*, 164–169.

Pang, R., Li, M., & Zhang, C. (2015). Degradation of phenolic compounds by laccase immobilized on carbon nanomaterials: Diffusional limitation investigation. *Talanta*, *131*, 38–45.

Park, A., & Oh, D. (2010). Effects of galactose and glucose on the hydrolysis reaction of a thermostable β-galactosidase from *Caldicellulosiruptor saccharolyticus*. *Applied Microbiology and Biotechnology*, *85*, 1427–1435.

Pavlidis, I. V., Patila, M., Bornscheuer, U. T., Gounis, D., & Stamatis, H. (2014). Graphene-based nanobiocatalytic systems: Recent advances and future prospects. *Trends in Biotechnology*, *32*, 6–21.

Pavlidis, I. V., Vorhaben, T., Tsoufis, T., Rudolf, P., Bornscheuer, U. T., Gournis, D., et al. (2012). Development of effective nanobiocatalytic systems through the immobilization of hydrolases on functionalized carbon-based nanomaterials. *Bioresource Technology*, *115*, 164–171.

Povedano, E., Cincotto, F. H., Parrado, C., Diez, P., Sanchez, A., Canevari, T. C., et al. (2017). Decoration of reduced graphene oxide with rhodium nanoparticles for the design

of a sensitive electrochemical enzyme biosensor for 17β-estradiol. *Biosensors and Bioelectronics*, *89*, 343–351.
Putzbach, W., & Ronkainen, N. J. (2013). Immobilization techniques in the fabrication of nanomaterial-based electrochemical biosensors: A review. *Sensors*, *13*, 4811–4840.
Rana, S., Yeh, Y. C., & Rotello, V. M. (2010). Engineering the nanoparticle–protein interface: Applications and possibilities. *Current Opinion in Chemical Biology*, *14*, 828–834.
Rezaei, A., Akhavan, O., Hashemi, E., & Shamsara, M. (2016). Ugi four-component assembly process: An efficient approach for one-pot multifunctionalization of nanographene oxide in water and its application in lipase immobilization. *Chemistry of Materials*, *28*, 3004–3016.
Romero, C. M., Pera, L. M., Loto, F., Vallejos, C., Castro, G., & Baigori, M. D. (2012). Purification of an organic solvent-tolerant lipase from *Aspergillus niger* MYA 135 and its application in ester synthesis. *Biocatalysis and Agricultural Biotechnology*, *1*, 25–31.
Rouhani, S., Rostani, A., Salimi, A., & Pourshiani, O. (2018). Graphene oxide/CuFe2O4 nanocomposite as a novel scaffold for the immobilization of laccase and its application as a recyclable nanobiocatalyst for the green synthesis of arylsulfonyl benzenediols. *Biochemical Engineering Journal*, *133*, 1–11.
Ruecha, N., Rangkupan, R., Rodthongkum, N., & Chailapakul, O. (2014). Novel paper-based cholesterol biosensor using graphene/polyvinylpyrrolidone/polyaniline nanocomposite. *Biosensors and Bioelectronics*, *52*, 13–19.
Sassolas, A., Blum, L. J., & Leca-Bouvier, B. D. (2012). Immobilization strategies to develop enzymatic biosensors. *Biotechnology Advances*, *30*, 489–511.
Sethuraman, V., Mthuraja, P., Anandha, R. J., & Manisankar, P. (2016). A highly sensitive electrochemical biosensor for catechol using conducting polymer reduced graphene oxide-metal oxide enzyme modified electrode. *Biosensors & Bioelectronics*, *84*, 112–129.
She, G. W., Huang, X., Jin, L. L., Qi, X. P., Mu, L. X., & Shi, W. S. (2014). Electrochemical sensors: SnO_2 nanoparticle-coated ZnO nanotube arrays for high-performance electrochemical sensors. *Small*, *10*, 4685–4692.
Shi, X. F., Xia, X. Y., Cui, G. W., Deng, N., Zhao, Y. Q., Zhuo, L. H., et al. (2015). Multiple exciton generation application of PbS quantum dots in ZnO@PbS/graphene oxide for enhanced photocatalytic activity. *Applied Catalysis B: Environmental*, *163*, 123–128.
Shin, H. J., Kim, K. K., Benayad, A., Yoon, S. M., Park, H. K., Jung, I. S., et al. (2009). Efficient reduction of graphite oxide by sodium borohydride and its effect on electrical conductance. *Advanced Functional Materials*, *19*, 1987–1992.
Singh, N., & Kayastha, A. M. (2012). Cicer α-galactosidase immobilization onto chitosan and Amberlite MB-150: Optimization, characterization, and its applications. *Carbohydrate Research*, *358*, 61–66.
Singh, N., Srivastava, G., Talat, M., Raghubhanshi, H., Srivastava, O. N., & Kayastha, A. M. (2014). Cicer α-galactosidase immobilization onto functionalized graphene nanosheets using response surface method and its applications. *Food Chemistry*, *142*, 430–438.
Song, J., Xu, L., Xing, R. Q., Li, Q. L., Zhou, C. Y., Liu, D. L., et al. (2014). Synthesis of Au/graphene oxide composites for selective and sensitive electrochemical detection of ascorbic acid. *Scientific Reports*, *4*, 7515. https://doi.org/10.1038/srep07515.
Sun, X., Liu, z., Welsher, k., Robinson, J. T., Goodwin, A., Zaric, S., et al. (2008). Nano-graphene oxide for cellular imaging and drug delivery. *Nano Research*, *1*, 203–212.
Sun, Z. Z., Yan, Z., Yao, J., Beitler, E., Zhu, Y., & Tour, J. M. (2010). Growth of graphene from solid carbon sources. *Nature*, *468*, 549–552.
Suplatov, D., Panin, N., Kirilin, E., Shcherbakova, T., Kudryavtsev, P., & Svedas, V. (2014). Computational design of a pH stable enzyme: Understanding molecular mechanism of penicillin acylase's adaptation to alkaline conditions. *PLoS One*, *9*, e100643.

Takahashi, S., Abiko, N., & Anzai, J. (2013). Redox response of reduced graphene oxide-modified glassy carbon electrodes to hydrogen peroxide and hydrazine. *Materials (Basel, Switzerland)*, *6*, 1840–1850.

Terse-Thakoor, T., Komori, K., Ramnani, P., Lee, I., & Mulchandani, A. (2015). Electrochemically functionalized seamless three-dimensional graphene–carbon nanotube hybrid for direct electron transfer of glucose oxidase and bioelectrocatalysis. *Langmuir*, *31*, 13054–13061.

Tian, J., Deng, S. Y., Li, D. L., Shan, D., He, W., Zhang, X. J., et al. (2013). Bioinspired polydopamine as the scaffold for the active AuNPs anchoring and the chemical simultaneously reduced graphene oxide: Characterization and the enhanced biosensing application. *Biosensors & Bioelectronics*, *49*, 466–471.

Tice, R. R., Agurell, E., Anderson, D., Burlinson, B., Hartmann, A., Kobayashi, H., et al. (2000). Single cell gel/comet assay: Guidelines for in vitro and in vivo genetic toxicology testing. *Environmental and Molecular Mutagenesis*, *35*, 206–221.

Venditti, I., Palocci, C., Chronopoulou, L., Fratoddi, I., Fontana, L., Diociaiuti, M., et al. (2015). *Candida rugosa* lipase immobilization on hydrophilic charged gold nanoparticles as promising biocatalysts: Activity and stability investigations. *Colloids and Surfaces B: Biointerfaces*, *131*, 93–101.

Verma, M. L., Barrow, C. J., & Puri, M. (2013). Nanobiotechnology as a novel paradigm for enzyme immobilization and stabilization with potential applications in biodiesel production. *Applied Microbiology and Biotechnology*, *97*, 23–39.

Vineh, M. B., Saboury, A. A., Poostchi, A. A., Rashidi, A. M., & Parivar, K. (2018). Stability and activity improvement of horseradish peroxidase by covalent immobilization on functionalized reduced graphene oxide and biodegradation of high phenol concentration. *International Journal of Biological Macromolecules*, *106*, 1314–1322.

Vnenchak, K. M., & Rokosz, K. (1997). The comet assay for detection of potential genotoxicity of polluted water. *Folia Biologica*, *45*, 153–239.

Walcarius, A., Minteer, S. D., Wang, J., Lin, Y., & Merkoci, A. (2013). Nanomaterials for bio-functionalized electrodes: Recent trends. *Journal of Materials Chemistry B*, *1*, 4878–4908.

Wang, Q., Cui, J., Li, G., Zhang, J., Li, D., Huang, F., et al. (2014). Laccase immobilized on a PAN/adsorbents composite nanofibrous membrane for catechol treatment by a biocatalysis/adsorption process. *Molecules*, *19*, 3376–3388.

Wang, Y., Li, Z., Wang, J., Li, J., & Lin, Y. (2011). Graphene and graphene oxide: Biofunctionalization and applications in biotechnology. *Trends in Biotechnology*, *29*, 205–212.

Wang, T., Liu, J., Ren, J., Wang, J., & Wang, E. (2015). Mimetic biomembrane-AuNPs-graphene hybrid as matrix for enzyme immobilization and bioelectrocatalysis study. *Talanta*, *143*, 438–441.

Wang, H., Zhang, Q., Chu, X., Chen, T., Ge, J., & Yu, R. (2011). Graphene oxide-peptide conjugate as an intracellular protease sensor for caspase-3 activation imaging in live cells. *Angewandte Chemie (International ed. in English)*, *50*, 7065–7069.

Wei, Z. Q., Wang, D. B., Kim, S., Kim, S. Y., Hu, Y. K., Yakes, M. K., et al. (2010). Nanoscale tunable reduction of graphene oxide for graphene electronics. *Science*, *11*, 1373–1376.

Xiao, P., Bu, F., Yang, G., Zhang, Y., & Xu, Y. (2017). Integration of graphene, nano sulfur, and conducting polymer into compact, flexible lithium–sulfur battery cathodes with ultrahigh volumetric capacity and superior cycling stability for foldable devices. *Advanced Materials, 29*. https://doi.org/10.1002/adma.201703324.

Xu, X. W., Shen, J. F., Li, N., & Ye, M. X. (2014). Facile synthesis of reduced graphene oxide/$CoWO_4$ nanocomposites with enhanced electrochemical performances for supercapacitors. *Electrochimica Acta*, *150*, 23–34.

Xu, J., Sheng, Z., Wang, X., Liu, X., Xia, J., Xiong, P., et al. (2016). Enhancement in ionic liquid tolerance of cellulase immobilized on PEGylated graphene oxide nanosheets: Application in saccharification of lignocellulose. *Bioresource Technology*, *200*, 1060–1074.

Yang, Y., Asiri, A. M., Du, D., & Lin, Y. (2014). Acetylcholinesterase biosensor based on a gold nanoparticle-polypyrrole-reduced graphene oxide nanocomposite modified electrode for the amperometric detection of organophosphorus pesticides. *Analyst*, *139*, 3055–3060.

Yang, K., Feng, L. Z., Hong, H., Cai, W. B., & Liu, Z. (2013). Preparation and functionalization of graphene nanocomposites for biomedical applications. *Nature Protocols*, *8*, 2392–2403.

Yang, W. R., Ratinac, K. R., Ringer, S. P., Thordarson, P., Gooding, J. J., & Braet, F. (2010). Carbon nanomaterials in biosensors: Should you use nanotubes or graphene? *Angewandte Chemie International Edition*, *49*, 2114–2138.

Yang, F. C., Wang, J., Cao, Y., Zhang, L., & Zhang, X. (2014). A highly sensitive ascorbic acid sensor based on carbon-supported CoPd nanoparticles. *Sensors and Actuators B: Chemical*, *205*, 20–25.

Yang, D., Wang, X., Shi, J., Wang, X., Zhang, S., Han, P., et al. (2016). In situ synthesized rGO–Fe_3O_4 nanocomposites as enzyme immobilization support for achieving high activity recovery and easy recycling. *Biochemical Engineering Journal*, *105*, 273–280.

Yang, H., Zhang, Y., Li, L., Sun, G., Zhang, L., Ge, S., et al. (2017). Real-time and in situ enzyme inhibition assay for the flux of hydrogen sulfide based on 3D interwoven AuPd-reduced graphene oxide network. *Biosensors & Bioelectronics*, *87*, 53–58.

Ye, X. L., Du, Y. L., Duan, K. Y., Lu, D. B., Wang, C. M., & Shi, X. Z. (2014). Fabrication of nano-ZnS coated PEDOT-reduced graphene oxide hybrids modified glassy carbon-rotating disk electrode and its application for simultaneous determination of adenine, guanine, and thymine. *Sensors and Actuators B: Chemical*, *203*, 271–281.

Yu, Y., Chen, Z., He, S., Zhang, B., Li, X., & Yao, M. (2014). Direct electron transfer of glucose oxidase and biosensing for glucose based on PDDA-capped gold nanoparticle modified graphene/multi-walled carbon nanotubes electrode. *Biosensors & Bioelectronics*, *52*, 147–152.

Yu, X., Cheng, H., Zhang, M., Zhao, Y., Qu, L., & Shi, G. (2017). Graphene-based smart materials. *Nature Reviews Materials*, *2*, 17046.

Yu, K. L. Q., Dong, K. T., Zhang, Y. P., Wang, Y. Q., & Zhi, Q. Q. (2014). Tuned n/n or n/p heterojunctions for reduced graphene oxide and titania nanosheets and their electrochemical properties. *Materials Chemistry and Physics*, *148*, 803–809.

Zhai, C., Guo, Y., Sun, X., Zheng, Y., & Wang, X. (2014). An acetylcholinesterase biosensor based on graphene-gold nanocomposite and calcined layered double hydroxide. *Enzyme and Microbial Technology*, *58–59*, 8–13.

Zhan, T. R., Tan, Z. W., Wang, X. J., & Hou, W. (2018). Hemoglobin immobilized in g-C3N4 nanoparticle decorated 3D graphene-LDH network: Direct electrochemistry and electrocatalysis to trichloroacetic acid. *Sensors and Actuators B: Chemical*, *255*, 149–158.

Zhang, J., Chen, S., Ruo, Y., Zhong, X., & Wu, X. (2015). An ultrasensitive electrochemiluminescent biosensor for the detection of concanavalin a based on poly(ethylenimine) reduced graphene oxide and hollow gold nanoparticles. *Analytical and Bioanalytical Chemistry*, *407*, 447–453.

Zhang, W., Li, X., Zou, R., Wu, H., Shi, H., Yu, S., et al. (2015). Multifunctional glucose biosensors from Fe_3O_4 nanoparticles modified chitosan/graphene nanocomposites. *Scientific Reports*, *5*, 11129–11138.

Zhang, Y., Shen, J., Li, H., Wang, L., Cao, D., Feng, X., et al. (2016). Recent progress on graphene-based electrochemical biosensors. *The Chemical Record*, *16*, 273–294.

Zheng, Y. L., Li, P., Li, H. B., & Chen, S. B. (2014). Controllable growth of cobalt oxide nanoparticles on reduced graphene oxide and its application for highly sensitive glucose sensor. *International Journal of Electrochemical Science*, *9*, 7369–7381.

Zhong, Z. Y., Li, M. X., Qing, Y., Dai, N., Guan, W., Liang, W., et al. (2014). Signal-on electrochemical immunoassay for APE1 using ionic liquid doped Au nanoparticle/graphene as a nanocarrier and alkaline phosphatase as enhancer. *Analyst*, *139*, 6563–6568.

Zhou, H. H., Han, G. Y., Fu, D. Y., Chang, Y. Z., Xiao, Y. M., & Zhai, H. J. (2014). Petal-shaped poly (3, 4-ethylenedioxythiophene)/sodium dodecyl sulfate-graphene oxide intercalation composites for high-performance electrochemical energy storage. *Journal of Power Sources*, *272*, 203–210.

Zhu, C. Z., & Dong, S. J. (2014). Energetic graphene-based electrochemical analytical devices in nucleic acid, protein and cancer diagnostics and detection. *Electroanalysis*, *26*, 14–29.

Zhu, C. Z., Du, D., & Lin, Y. H. (2017). Graphene-like 2D nanomaterial-based bio-interfaces for biosensing applications. *Biosensors and Bioelectronics*, *89*, 43–55.

Zhu, J., & Sun, G. (2012). Lipase immobilization on glutaraldehyde-activated nanofibrous membranes for improved enzyme stabilities and activities. *Reactive and Functional Polymers*, *72*, 839–845.

Zubir, N. A., Yacou, C., Motuzas, J., Zhang, X., Joao, C., & Costa, D. (2014). Structural and functional investigation of graphene oxide–Fe_3O_4 nanocomposites for the heterogeneous Fenton-like reaction. *Scientific Reports*, *4*, 4594.

FURTHER READING

Kim, J., Bayram, J., Park, C., Cheng, H., Dimitrakopoulos, C. W., Ott, C., et al. (2014). Principle of direct van der Waals epitaxy of single-crystalline films on epitaxial graphene. *Nature Communications*, *5*, 4836–4844.

Vigneshvar, S., Sudhakumari, C. C., Senthilkumaran, B., & Prakash, H. (2016). Recent advances in biosensor technology for potential applications—An overview. *Frontiers in Bioengineering and Biotechnology*, *4*, 3389.